Author Manuscript

Author Manuscript

Author Manuscript

Author Manuscript

HHS Public Access

Author manuscript

Sci Immunol. Author manuscript; available in PMC 2022 April 08.

Published in final edited form as:

Sci Immunol. 2022 February 04; 7(68): eabf6136. doi:10.1126/sciimmunol.abf6136.

Antigen cross-presentation in young tumor-bearing hosts promotes CD8+ T cell terminal differentiation

Ardiana Moustaki[1], **Jeremy Chase Crawford**[1], **Shanta Alli**[1], **Yiping Fan**[2], **Shannon Boi**[1], **Anthony E Zamora**[1], **Natalie M N McDonald**[1,5], **Gang Wu**[2], **Joy Nakitandwe**[3], **Scott Newman**[4], **Scott Foy**[4], **Antonina Silkov**[4], **Paul G Thomas**[1], **Alberto Pappo**[6], **Michael A Dyer**[7,8], **Elizabeth Stewart**[6,7], **Sara Federico**[6], **Ben Youngblood**[1,*]

[1]Department of Immunology, St. Jude Children's Research Hospital, Memphis, TN 38105, USA

[2]Center for Applied Bioinformatics, St. Jude Children's Research Hospital, Memphis, TN 38105, USA

[3]Department of Pathology, St. Jude Children's Research Hospital, Memphis, TN 38105, USA

[4]Department of Computational Biology, St. Jude Children's Research Hospital, Memphis, TN 38105, USA

[5]University of Tennessee Health and Science Center (UTHSC) - Memphis, TN 38163

[6]Department of Oncology, St. Jude Children's Research Hospital, Memphis, TN 38105, USA

[7]Department of Developmental Neurobiology, St. Jude Children's Research Hospital, Memphis, TN 38105, USA

[8]Department of Ophthalmology, University of Tennessee Health Science Center, Memphis, TN 38105, USA

Abstract

The immune system undergoes a progressive functional remodeling with age. Understanding how the age bias shapes anti-tumor immunity is essential in designing effective immunotherapies, especially for pediatric patients. In this manuscript we explore anti-tumor CD8+ T cell responses

*Correspondence: Benjamin.Youngblood@stjude.org.

Author contributions: based on the Contributor Roles Taxonomy (CRediT) guidelines (66):
A.M. performed conceptualization; methodology; investigation; writing – original draft; visualization and funding acquisition. J.C.C. performed methodology; formal analysis; data curation; visualization and writing – review and editing related to Fig. 5, Fig. 6A and Fig. S8B. S.A. performed investigation and validation. Y.F. performed methodology; formal analysis; data curation and visualization related to Fig. 6F. S.B. performed validation related to Fig. 2B. A.E.Z. performed investigation related to Fig. S8B; writing – review and editing and funding acquisition. N.M.N.M. performed validation related to Fig. 2B. G.W. performed formal analysis and supervision related to Fig. 6A. J.N. performed investigation related to Fig. 6A. S.N. performed formal analysis related to Fig. 6A. S.F. performed formal analysis related to Fig. 6A. A.S. performed formal analysis related to Fig. 6A. P.G.T. performed supervision and funding acquisition related to Fig. S8B. A.P. provided resources related to Fig. 6 and Fig. S8. M.A.D. provided resources related to Fig. 6 and Fig. S8, and performed writing – review and editing. E.S. provided resources and funding acquisition related to Fig. 6 and Fig. S8. S.F. provided resources and performed supervision related to Fig. 6 and Fig. S8. B.Y. performed conceptualization; writing – original draft; supervision and funding acquisition.

Competing interests: The authors declare that they have no competing interests.

Data and materials availability: The scRNAseq and WGBS data described in this manuscript have been deposited in NCBI's Gene Expression Omnibus (67) and are accessible through GEO Series accession number GSE188389. All other data needed to evaluate the conclusions in the paper are present in the paper or the Supplementary Materials. Request for reagents generated in this paper should be addressed to and will be fulfilled by the corresponding author upon a material transfer agreement.

Author Manuscript Author Manuscript Author Manuscript Author Manuscript

generated in young (prepubescent) and adult (pre-senescent) mice. Using an MHCI-deficient tumor model, we observed that tumor-reactive $CD8^+$ T cells expanded in young tumor-bearing (TB) mice acquired a terminally differentiated phenotype characterized by overexpression of inhibitory receptors and the transcription factor Tox1. Furthermore, tumor-infiltrating $CD8^+$ T cells from young tumors yielded a poor cytokine response compared to $CD8^+$ T cells infiltrating adult tumors. Young migratory dendritic cells (migDC) from the draining lymph nodes (dLNs), and mononuclear phagocytic cells (MPCs) infiltrating young tumors, were more competent in capturing and cross-presenting tumor antigen, leading to enhanced priming of $CD8^+$ T cells in dLNs, and their subsequent terminal differentiation in the tumors. Notably, single-cell transcriptional profiling of tumor infiltrating MPCs demonstrated that young MPCs are polarized toward an inflammatory, effector phenotype. Consistent with our observations in young vs adult TB mice, analysis of immune infiltrates from pediatric solid tumors showed a significant correlation between tumor-infiltrating $CD8^+$ T cells with an exhaustion phenotype and the frequency of PD-L1-expressing monocytes/macrophages. Collectively, these data indicate that a young tissue microenvironment contributes to the generation of an immune response skewed toward a less pliable terminal effector state, thus narrowing the window for immunotherapeutic interventions.

Keywords

T cell exhaustion; tumor microenvironment; age; antigen cross-presentation; pediatric tumors

Introduction

The specialized microenvironments where T cells differentiate and exert their effector functions undergo dynamic changes with age. The developmental plasticity of $CD8^+$ T cells allows them to adapt to these age-associated environmental changes in such a way that minimizes pathologic effects to the host. Communication of $CD8^+$ T cells with their microenvironment requires interaction of T cells with antigen-presenting cells (APCs) to ensure antigenic specificity. The strength of this interaction (TCR-pMHC), which is fine-tuned by the engagement of several accessory receptors and the presence of soluble factors, plays a central role in the differentiation of $CD8^+$ T cells (1, 2).

$CD8^+$ T cell differentiation in the context of chronic antigen exposure results in the generation of a heterogenous population of exhausted $CD8^+$ T cells (Tex) in terms of self-renewal and developmental plasticity (3-6). This cellular diversity is maintained by a pool of progenitor Tex cells characterized by increased expression of the transcription factor Tcf7 and decreased cytolytic activity (5, 7, 8). Persistent and strong TCR stimulation of the progenitor Tex cells triggers their expansion and differentiation toward a terminal state characterized by increased expression of several inhibitory receptors. The heightened level of inhibitory signals in the terminally differentiated $CD8^+$ T cells ensures their survival at the expense of their functionality. Tox1 has been identified as one of the major players in the generation and maintenance of exhausted $CD8^+$ T cells (9-13) that acts by mediating the TCR-induced expression of inhibitory receptors. Chronic stimulation epigenetically imprints the Tox locus for transcriptional activation, contributing so to the irreversible commitment of

Author Manuscript Author Manuscript Author Manuscript Author Manuscript

CD8$^+$ T cells to the exhausted state (12, 13). Notably, a subset of infiltrating CD8$^+$ T cells among various human cancers retain high levels of Tox expression (9-13). Based on these findings, Tox1 is currently considered a hallmark of T cell exhaustion.

Functional and numerical decline of T cells during advanced age is attributed not only to cell-intrinsic changes but also to extrinsic factors, including impaired function of dendritic cells in aged individuals that contribute to the poor stimulation of T cells (14-16). These findings would predict a superior immune function in children. While this seems to hold true in acute infections, as it is well established for the efficacy of vaccination (17), results from clinical trials in young cancer patients treated with immune checkpoint inhibitors (ICB) show inferior outcomes in this age group (18). The lack of responsiveness has been attributed to their low tumor mutational burden (TMB) compared to adult cancers (19, 20). However, this idea has been challenged by studies reporting that even a small number of neoantigens can trigger an efficient anti-tumor immune response (21, 22), suggesting that alternative mechanisms may restrict the endogenous T cell responses in children.

In this work, we explored how the differential ability of young and adult tumor-bearing hosts to cross-present tumor antigens affects CD8$^+$ T cell differentiation and function. We focused on the transition from childhood to adulthood to avoid confounding factors associated with the overall cellular and tissue degeneration observed in individuals of advanced age (23). To this end, we established an MHCI-deficient tumor model that expresses the GP33 LCMV epitope coupled to mCherry, enabling detailed analysis of anti-tumor T cell responses and characterization of antigen-presenting cells in the context of young versus adult hosts. We identified age-related changes in antigen uptake and cross-presentation that restrict polyfunctionality of CD8$^+$ T cells in tumor bearing young mice and skew their differentiation toward a terminally differentiated state. Finally, we analyzed immune infiltrates from human pediatric solid tumors and demonstrate that despite their low TMB pediatric solid tumors are enriched in antigen-experienced (PD1^{high}) CD8$^+$ T cells. Importantly, the exhaustion phenotype of these CD8$^+$ T cells (%PD1^{hi}Tim3$^+$) correlates with the frequency of PD-L1$^+$ myeloid cells in the TME of these tumors.

Results

Acquisition of a dysfunctional CD8 T cell state is enforced in the tumor microenvironment.

Tumors represent a distinct immunologic niche that can modulate the developmental trajectory of infiltrating effector CD8$^+$ T cells. Signals generated by the tumor cells or tumor stroma are relayed to CD8$^+$ T cells in an MHCI-restricted manner (24). To evaluate the effect of signals originating from the tumor microenvironment we used a transplantable mouse tumor model (MC38 cells) genetically modified to express a well-characterized T-cell epitope (GP33) and a fluorescent protein (mCherry) that enabled us to monitor tumor-specific T cell responses and antigen-bearing cells respectively.

Subcutaneous transplantation of MC38-GP33 tumor cells into immunocompetent, syngeneic hosts resulted in a massive expansion of the endogenous antigen-specific CD8$^+$ T cells (fig. S1, A-E) that are highly functional in peripheral lymphoid tissues (spleen and dLN) as manifested by the high percentage of cells capable of co-expressing IFNγ and IL-2 or TNFα

Author Manuscript Author Manuscript Author Manuscript Author Manuscript

during an *ex vivo* 4-hour restimulation assay with cognate peptide (GP33). However, the capacity of tumor-infiltrating GP33-specific $CD8^+$ T cells to recall expression of effector cytokines was significantly impaired. This tumor-associated suppression of $CD8^+$ T cells was observed in different tumor models (B16F10) and for different antigen specificities (NP396) (fig. S1F).

To assess whether the dysfunction of tumor-infiltrating $CD8^+$ T cells results from the selective infiltration of clonotypes with reduced functionality, we monitored the differentiation of a single GP33-specific T cell clone in an environment free of other competing clonotypes. For this study, we utilized $Rag1^{-/-}$ mice as TB hosts, and P14 transgenic $CD8^+$ T cells that express a TCR specific for the GP33 peptide (25) as tumor-specific T cells. MC38-GP33 tumors were established in $Rag1^{-/-}$ mice, and once they reached 200-300 mm^3 in volume, 5000 congenically marked ($CD90.1^+$) naïve P14 $CD8^+$ T cells were adoptively transferred into the TB mice (Fig. 1A). Similar to the endogenous response, we observed that tumor-infiltrating P14 cells were impaired in their ability to produce effector cytokines compared to the P14 cells from the spleens of the same mice (Fig. 1, B-D). These results confirmed the tumor-specific suppression of $CD8^+$ T cell function.

Having established that the dysfunction of tumor-specific $CD8^+$ T cells is a universal feature that occurs very early on during tumor development, we proceeded to investigate the cellular mechanisms involved in TME-associated $CD8^+$ T cell suppression. It is well documented that the suppression of tumor infiltrating $CD8^+$ T cells is antigen-specific (24). Apart from the tumor cells, tumor-infiltrating macrophages and DCs can also present tumor-derived antigens primarily through cross-presentation, in which extracellular antigens are internalized, processed, and loaded on MHCI molecules___. Indeed, using our $mCherry^+$ reporter tumor model, we identified a large proportion of the tumor immune infiltrates (almost entirely $CD11b^+$ myeloid cells) displaying mCherry fluorescence (fig. S2A), indicating that these cells had engulfed tumor-derived material and leading us to refer to them collectively as mononuclear phagocytic cells (MPCs). $mCherry^+CD11b^+$ MPCs were able to cross-present tumor antigen and activate naïve P14 $CD8^+$ T cells in an *ex vivo* antigen presentation assay as demonstrated by the upregulation of CD25 and CD69 markers (fig. S2, B and C).

The importance of the interaction between $CD8^+$ T cells and tumor-infiltrating MPCs has been shown in mouse tumor models where the efficacy of anti-PD-L1 immunotherapy is dependent on the expression of PD-L1 on host cells but not the tumor cells (26, 27). To focus on the interaction of $CD8^+$ T cells with the tumor-infiltrated antigen-presenting cells, we eliminated the crosstalk between $CD8^+$ T cells and tumor cells by knocking out the B2m gene in tumor cells (fig. S2, D and E). Despite the inability of the tumor cells to present antigen, the induction of the endogenous $CD8^+$ T cell response was comparable of that of the MHCI-proficient tumor cells (Fig. 1E). Abrogation of direct antigen presentation by tumor cells failed to restore the function of tumor-specific $CD8^+$ T cells in the TME (Fig. 1F, suggesting that cross-presentation of tumor antigens by non-tumor cells is sufficient to suppress $CD8^+$ T cell function.

Author Manuscript Author Manuscript Author Manuscript Author Manuscript

Young TME promotes differentiation of terminally differentiated CD8+ T cells

Age-associated differences in the function of DCs have been shown to affect adaptive immune responses against acute infections (14-16). However, the impact of aging innate immune cells in the context of persistent antigen exposure, observed during chronic infections and cancer, is not well-studied. Having established the contribution of TME in suppression of $CD8^+$ T cell function, we hypothesized that the age of the TME differentially affects the development of tumor-specific $CD8^+$ T cells.

To address our question, we compared differentiation of $CD8^+$ T cells generated in prepubescent young mice (4-weeks old) to $CD8^+$ T cells generated in mature-adult but not immune senescent mice (24-weeks old). To control for the age of the tumor-specific $CD8^+$ T cells we adoptively transferred naïve P14 $CD8^+$ T cells (8-12 weeks old) to both experimental groups prior to tumor challenge. The use of MHCI-deficient tumor cells ensured that only antigen presenting cells from the host can interact with the T cells (Fig. 2A). We refer to the P14 $CD8^+$ T cells generated in the young or adult TB hosts as "young-primed" or "adult-primed" respectively.

P14 $CD8^+$ T cells transferred into the young TB hosts expanded (Fig. 2B) and upregulated inhibitory receptors (PD1 and Tim3) (Fig. 2C) to a greater extent compared to P14 T cells transferred into adult hosts. The increased expression of inhibitory receptors indicates stronger TCR activation in the young hosts. Furthermore, measuring the expression of transcription factors downstream of TCR signaling (Nur77, Nfatc1, Irf4) provided additional evidence that the young-primed T cells received greater stimulation. To further assess the developmental trajectory of the P14 cells in the young versus adult animals, we measured the expression of Tox1. Young-primed P14 $CD8^+$ T cells expressed higher level of Tox1 (Fig. 2C), consistent Tox1 mediating the transduction of TCR signal to reduce expression of inhibitory receptor genes, a process that is crucial for the survival of the functionally exhausted $CD8^+$ T cells (9-13).

Subsequently, we assessed whether the age-related discrepancies in the activation of $CD8^+$ T cells were translated to changes in the effector function of these tumor-specific $CD8^+$ T cells. Our work showed that the microenvironment of even a newly established tumor can suppress the ability of $CD8^+$ T cells to secrete effector molecules though these cells are highly functional in peripheral lymphoid organs (Fig. 1; fig. S1). While this tumor-specific suppression was observed in both young and adult mice, the age of the host greatly impacted the functionality of the tumor-infiltrating $CD8^+$ T cells: P14 cells isolated from adult tumors demonstrated a higher ability to produce IFNg along with IL-2 and/or TNFα, when compared to cells from young tumors (Fig. 2D). We also confirmed that the enhanced activation and expansion of the young-primed P14 $CD8^+$ T cells also occurred in the less immunogenic B16-F10 melanoma tumor model (fig. S3B). These results indicate that the adult TME establishes a setting that is less immunosuppressive for tumor-specific T cells relative to a young TME.

To validate whether the observed age-associated differences also occur in other contexts of chronic antigen exposure, we analyzed the early differentiation of naïve P14 $CD8^+$ T cells in young vs adult mice chronically infected with LCMV Cl13 (fig. S4A). Similar to the tumor

Author Manuscript Author Manuscript Author Manuscript Author Manuscript

model, the young-primed P14 cells upregulated expression of Tox1 and PD1 to a greater extent (fig. S4B). Interestingly, the excessive activation of T cells in the young mice was coupled with a sharp contraction of the splenic T cell compartment as manifested by the pronounced cell death of total splenocytes and specifically of the P14 $CD8^+$ T cells in the young hosts (fig. S4, C and D). Consistent with increased activation-induced cell death, the number of total P14 cells was significantly reduced in the spleens of young mice compared to the adult (fig. S4E). Like the tumor-specific T cells, the young-primed P14 cells exhibited an impaired cytokine response upon *ex vivo* stimulation with the cognate peptide (fig. S4F), which was associated with higher viral titers in the plasma of the young mice (fig. S4G). The results from the viral infection model support the idea that the hyperactive $CD8^+$ T cells generated in young hosts rapidly acquire a terminally differentiated phenotype with a reduced capacity to express effector cytokines.

The results from the above-described models demonstrate that age-associated differences are established early during $CD8^+$ T cell development in the peripheral lymphoid tissues. To determine if these age-associated changes impact on the T cell's effector potential, we tested the T cell's ability to respond to secondary antigenic challenge in two different models. Initially, we adoptively transferred young- or adult-primed splenic P14 $CD8^+$ T cells from TB mice (day 7) to naïve secondary hosts of the same age (8-weeks old) (fig. S5A), which were subsequently challenged with an acute LCMV infection. The systemic LCMV challenge ensures high antigen load throughout the internal organs of the mice. We observed that the young-primed P14 cells retained their proliferative advantage compared with the adult-primed cells (fig. S5B). Next, to test their ability to control tumor growth, we transferred young- or adult-primed splenic P14 cells into NSG mice bearing established MC38-GP33 tumors (fig. S5C). Immunodeficient mice were used to avoid the endogenous anti-tumor response which is stronger compared to the transferred P14 effector cells. While P14 cells from both age groups were initially able to expand and control the rate of tumor growth, the adult-primed P14 cells exhibited greater control after a longer period (fig. S5, D-G).

Collectively our data demonstrate that antigen-specific $CD8^+$ T cells generated in the peripheral lymphoid organs of young hosts show a hyperactivated, effector phenotype that is coupled to an exacerbation of their functional exhaustion in the context of high antigen load (i.e., in the tumor). To gain insight into the underlying mechanisms of these age-related differences, we subsequently focused on the innate arm of the immune system, which is crucial for initiation and maintenance of the adaptive immune responses. We explored the properties of the MPCs that mediate the initial priming of antigen-specific $CD8^+$ T cells in the draining lymph nodes, as well as the MPCs that reside in the established tumors.

Heightened antigen cross-presentation by young migratory DCs is associated with enhanced priming of $CD8^+$ T cells in the tumor dLNs

The initial priming of $CD8^+$ T cells has a profound effect on the magnitude of $CD8^+$ T cell expansion and their subsequent differentiation (28, 29). Successful activation of T cells depends on the functional maturation of APCs, a process that is marked by expression of co-stimulatory molecules following internalization of antigens (30, 31). Efferocytosis, the

Author Manuscript Author Manuscript Author Manuscript Author Manuscript

removal of apoptotic cells by MPCs, is the primary process by which tumor antigens spread to the draining lymph nodes and trigger systemic anti-tumor immunity (32).

In order to examine the antigen-presenting potential of host MPCs___, we inoculated young and adult mice subcutaneously with apoptotic MHCI-deficient MC38-GP33 tumor cells, and the next day assessed the presence of mCherry^{+} cells in the inguinal dLNs (Fig. 3A). The vast majority of cells that were positive for tumor-derived mCherry at 18h after tumor cell injection were migratory DCs (migDCs; Lin^{-}Ly6G^{-}CD11c^{int}MHCII^{hi}) (Fig. 3B) in both age groups; however, we observed an increase in the percentage of inflammatory monocytes (iMo; Lin^{-}CD11b^{+}Ly6G^{-}Ly6C^{+}MHCII^{+}) in the adult cohort most likely reflecting direct lymphatic delivery of tumor antigens in the older mice (fig. S6A). The mCherry^{+} migDCs from the dLNs of the young mice expressed higher levels of the LN-homing receptor Ccr7 (33) and lower levels of the β2-integrin CD11c, which has been shown to anchor DCs at the site of inflammation (34) (Fig. 3D; fig. S6B). This suggests decreased migratory potential of the DCs from the periphery to the LN, which is consistent with the lower number of mCherry^{+} cells in the dLNs of the adult mice (Fig. 3C). Moreover, young migDCs had a more activated and mature phenotype as demonstrated by higher expression of co-stimulatory molecules (CD80, CD86) and MHCII surface molecules (Fig. 3D; fig. S6B). In contrast, the adult mCherry^{+} migDCs exhibited a less mature phenotype and also expressed higher levels of the ligand for the T cell inhibitory receptor PD1 (PD-L1), which has been shown to inhibit proliferation of T cells (35, 36).

Similar results were obtained when we assessed the capture and transfer of soluble antigen in young mice. Subcutaneous administration of CFA-adjuvanted fluorescent OVA protein revealed four main cell populations in the dLNs that had captured antigen: neutrophils, iMo, resident DCs (rDC; Lin^{-} Ly6G^{-}CD11c^{hi}MHCII^{int}), and migDC, with iMo and migDCs being the predominant cell types (fig. S6C). The expression density of maturation markers (MHCII, CD86 and CD40) was higher on the surface of migDCs from young dLNs (fig. S6E). These results indicate that not only is there an antigen abundance in the dLN of young mice, but the young DC subsets have a phenotype indicative of greater potential to cross-present antigen and activate T cells.

To further characterize cross-presentation of tumor antigens in young mice, we monitored the proliferation of P14 CD8^{+} T cells during their early encounter with tumor antigen in the dLNs. P14 cells were labeled with cell trace violet dye and adoptively transferred into mice, which were subsequently challenged with MHCI-deficient MC38-GP33 cells. Notably, three days post-tumor challenge, proliferating P14 CD8^{+} T cells were exclusively detected in the dLNs. The precursor frequency of P14 cells that divided at least once, and the average number of successful divisions completed by the proliferating cells, were significantly higher when the T cells were activated in the young hosts (Fig. 3E). Moreover, the undivided fraction of the young-primed P14 cells expressed higher level of inhibitory receptors (PD1 and Tim3), Nfat, Irf4, CD25 and CD69 (Fig. 3F), indicating that the transferred cells experienced greater TCR-mediated stimulation. Once the young-primed P14 cells entered the cell cycle, they differentiated further down the effector developmental path as manifested by the decreased density of TCR complexes on their surface, the rapid downregulation of CD69. The same enhanced proliferation of P14 cells was observed in the dLN of young

Author Manuscript Author Manuscript Author Manuscript Author Manuscript

mice challenged with B16F10-BKO-GP33 tumor cells (fig. S3A). Overall, these results document that age-associated differences in activation and maturation of MPCs can have a profound effect in stimulation and expansion of $CD8^+$ T cells.

Tumor infiltrating MPCs from young mice are more efficient in cross-presenting tumor antigen to $CD8^+$ T cells

The above-described difference in the initial priming of T cells does not fully account for the reduced functionality of tumor infiltrating T cells in young hosts, since $CD8^+$ T cells in peripheral tissues of both age groups were highly functional (fig. S7A). Therefore, we hypothesized that age-related differences in the MPCs residing in the tumors are also likely linked to the increased suppression of $CD8^+$ T cells in the young mice.

We identified tumor-infiltrating mononuclear cells as the main cell population that uptake tumor proteins (fig. S7B). A significant percentage of MPCs expressed the Ly6C marker indicative of their monocytic lineage. Indeed, tumors recruit BM-derived monocytes that upon infiltration in the tumor tissue acquire an inflammatory phenotype [iMo: inflammatory monocytes; also referred to as TipDC (TNF and iNOS producing DCs) or iDCs (inflammatory DCs)] and further differentiate into macrophages (37). Similar developmental stages were observed in our tumor model, where the transition of monocytes to macrophages was characterized by an increase in tumor antigen uptake and surface expression of PD-L1 (Fig. S7D). We didn't observe any age-related perturbation of this differentiation process as indicated by the comparable percentage of tumor infiltrating MPCs and their similar cellular composition between the young and adult TB hosts (Fig. S7E).

However, tumor infiltrating MPCs from young mice were more proficient in taking up tumor proteins, as evidenced by the increased frequency of $mCherry^+$ cells and the higher intensity of mCherry marker at the single-cell level (Fig. 4A). Similarly, this was observed in our B16F10-BKO-GP33 tumor model, although the melanoma cells appeared to be more resistant to phagocytosis, as evidenced by the lower frequency of mCherry+ cells and reduced MFI (fig. S3C). Young MPCs demonstrated a more mature phenotype with increased expression of MHC molecules, activation, and maturation markers (Fig. 4B; fig. S7C). However, the young MPCs also co-expressed higher levels of the ligand for the inhibitory receptor PD1 (PD-L1).

To directly test if the young tumor-infiltrating MPCs are more efficient at cross-presenting antigen, we used $CD11b^+$cells isolated from young and adult MC38-BKO-GP33 tumors to stimulate naïve P14 $CD8^+$ T cells *ex vivo*, after normalizing for the number of $mCherry^+CD11b^+$ cells (Fig. 4C; fig. S7F). Young MPCs were able to better activate P14 cells, as shown by the increased frequency of cells expressing CD25 and CD69 (Fig. 4D). Moreover, these activated cells showed higher expression levels of TCR downstream target molecules (PD1, Nfatc1, Nur77) when cocultured with young MPCs (Fig. 4D). However, we didn't observe any difference in the proliferation of P14 cells 3 days after *ex vivo* stimulation (fig. S7H), presumably due to inherent limitation of the assay that doesn't allow for prolonged antigen exposure, as shown by the rapid turnover of the TCR after the second division (fig. S7I).

Author Manuscript Author Manuscript Author Manuscript Author Manuscript

The host age diversifies the tumor infiltrating MPCs into distinct activation states.

To further profile tumor-infiltrating MPCs, we isolated total mCherry$^+$ cells from MC38-GP33-BKO tumors established in young or adult mice and analyzed their transcriptomes at the single-cell level (Fig. 5A). Unsupervised gene expression analysis of mCherry$^+$ cells broadly revealed clusters that corresponded to tumor cells (3.94%), neutrophils (3.09%), lymphocytes (1.5%), and a composite of MPCs (84.43%) (Fig. 5B and 5C). Comparison of cells obtained from young versus adult hosts showed a uniform mixing among the tumor cells; however, MPCs demonstrated substantial heterogeneity in gene expression signatures that largely corresponding to host age (Fig. 5D). Gene ontology and pathway enrichment analysis indicated that, relative to those from the adult host, MPCs from the young TB hosts upregulated processes involved in cross-presentation of extracellular proteins including the endosomal/vacuolar pathway, the ER-Phagosome pathway, antigen presentation, trafficking, and processing of endosomal Toll-Like Receptors (Fig. 5E). This gene signature is consistent with the more stimulatory phenotype we observed in the young MPCs (Fig. 4B).

Interestingly, genes commonly associated with the activation of macrophages toward a pro-inflammatory (classically activated, effector macrophages) or anti-inflammatory (alternatively activated, wound healing macrophages) state also exhibited distinct patterns across the two age groups, with the former often expressed in greater abundances among cells from the young host (Fig. 5E and 5F). The inducible nitric oxide synthase (iNOS or NOS2), the hallmark enzyme of classically activated macrophages (38, 39), is expressed mostly by young MPCs as depicted by the increased frequency of expressing cells as well as higher expression on a per cell basis. Similarly, the hallmark enzyme of alternatively activated macrophages, arginase (Arg), was expressed by the majority of MPCs but at higher levels by the adult MPCs. A metabolic shift toward ribosomal biogenesis was observed in adult MPCs as manifested by the increased expression of genes encoding for ribosomal proteins (Fig. 5E). Although regulation of translational machinery in macrophages is an underexplored area, polarized synthesis of rRNA has been described in peritoneal macrophages activated toward a cytotoxic or immunosuppressive phenotype (40). Collectively, these data suggest that persistent stimulation of CD8$^+$ T cells by pro-inflammatory MPCs, which are characterized by enhanced phagocytic and antigen cross-presentation activity, is associated with the functional exhaustion of the tumor-infiltrating T cells.

CD8$^+$ T cells infiltrating pediatric solid tumors are enriched with antigen experienced PD1hi cells.

Cumulatively, the studies described thus far document a strong difference in T cell differentiation that is coupled to the age of the TB hosts. This observation prompted us to look for evidence of a comparable mechanism for CD8$^+$ T cell suppression in human pediatric tumors. We examined a collection of 83 pediatric solid tumor specimens, comprising 34 different tumor types, from children and adolescent patients enrolled in the MAST protocol (41). Whole exome sequencing data were available for a subset (n=23) of these samples and were used to calculate the mutation rate (Fig. 6A). As expected, the mutation rate of the samples used in this study were comparable to common pediatric

Author Manuscript Author Manuscript Author Manuscript Author Manuscript

tumors previously published as a part of the Pediatric Cancer Genome Project(42). Based on their low mutation burden, pediatric tumors are conceived to be poorly immunogenic. However, immunophenotypic characterization of these tumors revealed that the infiltrating $CD8^+$ T cells showed an effector-memory phenotype ($CCR7^-CD45RO^{+/-}$) (Fig. 6D) that was associated with a wide range of PD1 expression among all tumor types (Fig. 6B). Compared to $CD8^+$ T cells from the peripheral blood (PB) of healthy individuals, almost all tumor samples were enriched with $PD1^{int}$ and $PD1^{hi}$ $CD8^+$ T cells (Fig. 6C), suggesting the persistent presence of their cognate antigen (43). To indirectly assess whether the enrichment for a $PD1^{hi}$ phenotype in these tumors occurs via an antigen-dependent manner, we evaluated the diversity of the T cell receptor (TCR) repertoire of $CD8^+$ T cells with high (co-expressing TIM3), intermediate, and low PD1 expression levels by using single-cell TCR sequencing (fig. S8B). $CD8^+$ TILs co-expressing PD1 and TIM3 were enriched in clonally expanded TCRαβ clonotypes, suggesting that T cells undergo a hierarchal clonal selection as they commit to more differentiated cell states. The presence of dominant clonotypes (i.e., the same TCR shared among many T cells) has been previously associated with expansion of neoantigen-specific $CD8^+$ T cells (44, 45). Overall, these results indicate that pediatric solid tumors can trigger anti-tumor immune responses, generating a pool of antigen-experienced $CD8^+$ T cells that could be a potential target for immunotherapy.

The frequency of PD-L1-expressing macrophages from pediatric solid tumors is coupled to $CD8^+$ T cell exhaustion phenotype.

Following our observations from mouse tumor models, we sought to explore whether the magnitude of antigen cross-presentation by the tumor infiltrating MPCs is linked with exhaustion of $CD8^+$ TILs. The coexpression of inhibitory receptors by $CD8^+$ TILs is commonly used to describe exhausted $CD8^+$ T cells. However inhibitory receptors are not expressed exclusively during the exhaustion phase of T cell differentiation: PD1, TIM3 and CD39 are similarly upregulated during the acute phase of an infection in effector $CD8^+$ T cells, which are highly functional. To assess whether pediatric $PD1^{high}$ $CD8^+$ TILs had acquired features of T cell exhaustion, we assessed the expression of TOX1 and TCF7, two transcription factors that regulate differentiation and maintenance of exhausted $CD8^+$ T cells (5, 7, 10-13). TOX1 was highly upregulated in $PD1^{high}CD39^+$ $CD8^+$ TILs while the $PD1^{int}$ and $PD1^{low}$ $CD8^+$ TILs retained a lower level of TOX1 expression comparable to naïve $CD8^+$ T cells from peripheral blood (PB) of healthy donors (HD) (Fig. 6E). In contrast, the expression of TCF7 followed a reverse pattern with the $PD1^{high}CD39^+$ $CD8^+$ TILs showing pronounced downregulation compared to naïve $CD8^+$ T cells, further confirming that $CD8^+$ TILs with a high density of inhibitory receptors on their cell surface are skewed toward a terminal differentiation stage. Additionally, we found that the human TOX1 gene locus is demethylated in $PD1^+$ tumor-infiltrating $CD8^+$ T cells, while it is completely methylated in $PD1^-$ $CD8^+$ TILs and naïve $CD8^+$ T cells isolated from HD-PB (Fig. 6F). Demethylation of the Tox1 locus has been reported to enforce persistent gene expression during chronic viral infection (13). Collectively, our phenotypic and epigenetic data indicate that pediatric $PD1^{hi}CD39^+$ TILs undergo developmental changes that drive them toward a state of T cell exhaustion that has limited developmental potential.

Author Manuscript Author Manuscript Author Manuscript Author Manuscript

Lacking a feasible methodology to directly measure antigen cross-presentation in human tumors, we exploited our previous observation on the mouse tumor model that the ability of tumor infiltrating MPCs to capture antigens is directly correlated with the surface expression of the PD-L1 inhibitory ligand (fig. S7C). Using PD-L1 as a surrogate marker for identifying MPCs, we initially noted that PD-L1 expression was predominantly limited to the $CD45^+$ fraction of the cells (Fig. 6G), and that monocytes and macrophages were the major cell types with high levels of PD-L1 expression (Fig. 6H), consistent with prior reports (46). Clustering of pediatric samples based on the frequency of the $PD1^{high}$ $CD8^+$ T cells that co-express TIM3 identified a significant correlation with the expression of PD-L1 by the macrophages. Specifically, tumors containing $CD8^+$ T cells with high TIM3 expression (>20% among $PD1^{high}$) were more likely to be enriched for myeloid cells that express high level of PD-L1 (Fig. 6I). To explore the possibility of an age bias in the establishment of the exhausted phenotype we focused on neuroblastoma samples, which spread across a wider age spectrum. We observed that the exhausted phenotype (%$TIM3^+$ PD^{high} $CD8^+$ TILs) and the phagocytic activity of tumor stroma (% PD-L1 expressing macrophages) was trending higher in the 2-10 years old age group (fig. S7D), however a larger dataset is needed to power this analysis for statistical conclusions. These results support our observations in mice that the interaction between $CD8^+$ TILs and the myeloid cells in the tumor stroma represent a potential mechanism that skews $CD8^+$ T cells toward a fully exhausted differentiation program.

Collectively our findings indicate that the “immature” microenvironment of an actively developing individual favors the terminal differentiation of $CD8^+$ T cells under conditions of persistent antigen exposure. In tumor settings, the exacerbated functional exhaustion of $CD8^+$ T cells in young individuals likely contributes to the weakened anti-tumor immunity observed in children. Our findings provide insights not only in our fundamental understanding of the immune system during aging but also for our efforts to optimize immunotherapeutic interventions.

Discussion

Several studies in the past decade have established that generation of a heterogenous population of $CD8^+$ T cells during chronic pathogenic threats is important in maintaining a long lasting – although functionally impaired – immunity (5, 7, 10-13). In light of these findings, exploring the factors that modulate the fate of $CD8^+$ T cell development is important in understanding and overcoming the limitations of our immune system. Here we show how the age of an organism can greatly influence the cell fate potential of antigen-specific T cells as they undergo effector differentiation. We emphasize that changes even within a narrower developmental window, like that between adolescence and early adulthood, can have a profound effect on how our immune system is primed and adapts to infections or transformed cells.

Although innate immunity is indispensable for activation and maintenance of adaptive immune responses, the effects of an ageing innate immune system on the development of T cells haven’t been explored proportionally. However, several studies have concluded that the function of APCs (either DC or macrophages) declines with advanced age (16, 47, 48):

Author Manuscript Author Manuscript Author Manuscript Author Manuscript

impaired phagocytosis and responsiveness to external stimuli lead to reduced expression of MHC molecules and several co-stimulatory proteins. Our results from adult mice indicate a similar reduction in the ability of migDCs in the dLNs and MPCs in the tumors to take up and cross-present tumor antigens. However, we demonstrate that in settings of persistent antigen exposure the enhanced stimulation of CD8 T cells by myeloid cells leads to their rapid exhaustion and terminal differentiation.

More specifically, tumor-reactive $CD8^+$ T cells expanding in young TB hosts acquire a terminally differentiated phenotype and exhibit a pronounced exhaustion profile in the presence of high antigen load such as the one that occurs in the TME or certain chronic viral infections. We observed that the antigen-bearing ($mCherry^+$) MPCs from adult tumors were polarized toward an immunosuppressive M2-like phenotype, while MPCs from young tumors were polarized toward a pro-inflammatory M1-like phenotype. Immunosuppressive macrophages have long been considered to exert their pro-tumorigenic effects among others by suppressing $CD8^+$ T cell function (49). Surprisingly though, $CD8^+$ T cells infiltrating adult tumors demonstrated an increased cytokine response compared to $CD8^+$ TILs from young tumors despite the presence of macrophages with a more immunosuppressive phenotype. The observed discrepancy in the polarization of MPCs and the functionality of tumor-specific-$CD8^+$ T cells could be explained by the greater ability of young MPCs to uptake tumor proteins compared to the adult cells, which is consistent with the fact that M1-macrophages are highly phagocytic (50). The abundance of tumor antigen cross-presented by the young MPCs results in excessive activation of $CD8^+$ T cells, forcing T cells further down the exhaustion differentiation pathway. Accordingly, the low availability of MHCI-presented tumor antigen in the adult tumors is associated with increased functionality of $CD8^+$ T cells.

Moreover, our data suggest that the fate of $CD8^+$ T cells can be skewed before they infiltrate the tumors. Young-primed $CD8^+$ T cells from the dLNs were highly proliferative and activated even before entering the systemic circulation (day 3 after tumor challenge). This was associated with the increased activation and maturation profile of migratory DCs in the young hosts. While the enhanced effector profile acquired during the initial priming of $CD8^+$ T cells might lead to a rapid clonal expansion, at the same time restrains their developmental potential toward a terminal state in the context of persistent antigen exposure. These results suggest that the innate arm of a young immune system skews the differentiation of $CD8^+$ T cells toward a terminal stage with limited developmental plasticity. While the generation of less plastic cells may seem counterintuitive for the establishment of immunological memory, from an evolutionary point of view, we can speculate that a powerful effector T cell response early in life, although less pliable, confers a survival advantage for the host who encounters a plethora of pathogens for the first time. Later in life, predominance of type-2 immunity, which counteracts the immunopathology caused by the effector/cytotoxic (type-1) responses, is considered beneficial for the host.

There are examples in the literature that corroborate the hypothesis of the age-bias on the differentiation niche of $CD8^+$ T cells. For instance, it has been shown that neonatal $CD8^+$ T cells expand more rapidly and give rise to terminally differentiated effector cells, when challenged with *Listeria monocytogene* (LM), an intracellular bacterium that

Author Manuscript Author Manuscript Author Manuscript Author Manuscript

causes acute infection (51). Another example in support of the Th1 immune bias in young individuals comes from an experimental model of multiple sclerosis (MS), where it was shown that the susceptibility to experimental autoimmune encephalomyelitis (EAE) in mice drops dramatically after 4 weeks of age (puberty) despite the fact that the numbers of myelin-specific CD4 T cells and the amount of antigen remains stable after 4 weeks (52). The polarization of the immune response based on age was more recently reported in patients with classical Hodgkin lymphoma (cHL); a tolerogenic TME comprised of M2-macrophages and Tregs was predominant in cHL patients older than 10 years, whereas M1-type macrophages were prevalent in cHL patients younger than 10 years (53). More importantly, the pro-inflammatory phenotype of macrophages in the younger pediatric patients was associated with an increased percentage of Granzyme B positive cells.

Finally, by profiling the immune infiltrates from pediatric solid tumors we provide evidence that a similar mechanism of premature exhaustion of T cells may restrict the endogenous anti-tumor T cell responses in children. Initially, we established that pediatric solid tumors are enriched in antigen-experienced $CD8^+$ T cells despite their low TMB. This observation is in line with a report on ALL where the authors could detect tumor-associated $CD8^+$ T cells reactive to 86% of predictive neo-epitopes for each tumor tested (21). However, in our dataset we observed that tumors enriched in $CD8^+$ T cells with an exhausted phenotype are more likely to have a high percentage of PD-$L1^+$ myeloid cells, which reflected phagocytic myeloid cells in our mouse models. This suggest that tumor infiltrating APCs are associated with and could promote $CD8^+$ T cell dysfunction in pediatric tumors.

Although we cannot draw definitive conclusions from the human pediatric cohort due to the diverse origin of tumor types and the rare occurrence of pediatric tumors, our data highlight the need for clinical trials designed to address age-related differences in anti-tumor adaptive and innate immunity. A side-by-side comparison of adult vs pediatric tumors controlled for confounding factors (e.g. tumor type or tissue of origin, mutational burden, treatment regimen) would provide more compelling evidence on the role of immune intrinsic factors in anti-tumor immunity. This, evidently, will require collaboration of multiple pediatric centers in order to gather a sample size with significant statistical power. Another limitation highlighted by our studies is that investigation of T cell biology in human subjects relies on expression of surrogate markers even though T cell differentiation is TCR-centered, MHC-restricted, and antigen-specific. This is mainly due to lack of methodologies for identifying and validating tumor antigens in a time- and cost-efficient manner. Given the remarkable success of T-cell based immunotherapies in the past decade, we would like to urge the research community to prioritize functional studies of T cells in clinical trials.

Broadly, the results described here emphasize the age of an individual as an important factor in the design of immunotherapeutic approaches. Understandably, current T cell-based immunotherapy approaches are based largely on our knowledge of the adult immune system, however given the relatively limited investigation of the pediatric immune system, interpretation of results that come from pediatric immunotherapy studies may need to be tempered. While a full understanding of the mechanisms that favor the terminal differentiation of anti-tumor T cells in pediatric solid tumors remains to be elucidated,

Author Manuscript Author Manuscript Author Manuscript Author Manuscript

our work provides a conceptual foundation for exploring the specific characteristics of the pediatric immune system and their role in shaping the antitumor T cell response in children.

Material and Methods

Study design

The objective of this study was to investigate the role of age of the host APCs on the interaction of $CD8^+$ T cells with the APCs. For this we evaluated (*a*) the CD8 T cell response (activation, proliferation differentiation, and function), and (*b*) the ability of APCs to cross-present tumor antigen and their overall maturation state, during (*c*) the early activation phase (day 3) that takes place in the dLNs, and (*d*) late differentiation of T cells in the tumors. The mouse studies were complemented by immunophenotyping of CD8 T cells infiltrating pediatric solid tumors. The sample size for mouse experiments with no previous experience was determined using statistical power analysis (GPower 3.1 tool) (54, 55). TB mice used in the rechallenge experiments (fig. S5C) were distributed into the 2 age groups based on a randomized block design after removal of outliers (ROUT method). All mouse experiments were performed with 5-10 biological replicates per experimental group. All experiments were repeated at least twice unless otherwise stated.

Human samples

Blood samples: De-identified blood samples were obtained as plateletpheresis byproducts from healthy individuals through the St Jude Blood Donor Center. Peripheral blood mononuclear cells (PBMC) were isolated by Ficoll-Hypaque (GE Healthcare) density centrifugation using standard procedures.

Tumor samples: De-identified, freshly resected surgical specimen were obtained from pediatric patients consented to participate in the MAST protocol (NCT01050296), in agreement with local institutional ethical regulations and institutional review board approval (IRB protocol XPD09-234). All tumor samples were processed and analyzed fresh.

Somatic coding mutation analysis

Somatic mutations were curated for MAST tumors as part of the St. Jude Children's Research Hospital Clinical Genomics process. Whole-exome sequencing and subsequent analysis was performed on both germline and tumor sample from each patient as described by Rusch et al 2018 (56). Mutation rates were calculated relative to the number of sequenced coding bases with at least 10x coverage per sample in each germline-tumor pair. For comparison to other pediatric tumors, mutation rates were also included from published data obtained from the St. Jude Children's Research Hospital/Washington University Pediatric Cancer Genome Project (PCGP) (42).

Animals

C56Bl/6J mice were purchased from The Jackson Laboratory (Jax; Stock No: 000664). The immunodeficient Rag1KO mice (Stock No: 002216), NSG (Stock No: 005557) and the B2mKO mice (Stock No: 002087) were purchased from Jax and bred in house. The P14 TCR transgenic mouse line, a generous gift from Dr David Masopust, was backcrossed into

Author Manuscript Author Manuscript Author Manuscript Author Manuscript

a C57Bl/6 Thy1.1 background (Jax Stock No: 000406). For all *in vivo* experiments, except the ageing studies, 8-12-weeks old mice were used. Mice allocated to different experimental groups were sex-, age-, and housing-matched. Female mice were used throughout the study. All animal studies were performed in accordance with the recommendations in the *Guide for the Care and Use of Laboratory Animals* (the Guide) of the National Institutes of Health. Animal protocols were approved on an annual term by the Institutional Animal Care and Use Committee (IACUC; protocol #: 598-100569) at St. Jude Children's Research Hospital.

Cell lines and generation of transgenic cell lines

The mouse colon adenocarcinoma cell line, MC38 (H-2b haplotype), curtesy of Dr. Hongbo Chi (SJCRH), was maintained in high glucose DMEM medium (Gibco) supplemented with 10% FBS (Hyclone) and antibiotics (Gibco, penicillin 100U/mL, streptomycin 100 μg/mL). The mouse melanoma cell line, B16F10 (H-2b) was purchased from ATCC (CRL-6475) and was maintained in ATCC-modified RPMI 1640 medium (Gibco) supplemented with 10% FBS and Pen/Strep. The HEK293T cell line was purchased from ATCC (CRL-3216) and maintained in high glucose DMEM medium (Gibco) supplemented with 10% FBS and Pen/Strep. All cell lines were maintained at 37°C in humidified air with 5% CO_2.

The immunogenic cell lines were generated by lentiviral transduction and subsequent FACS sorting of $mCherry^+$ cells spreading within a narrow window of fluorescence intensity (low CV). All transgenic cell lines used in this study are polyclonal to dilute-out potential artifacts due to insertional mutagenic effects.

To knock out the B2m gene, MC38 cells were transiently transfected with the Crispr vector. Crispr/Cas9 edits were introduced through the non-homologous end joining pathway targeting 3 different gene regions (crRNA1: ATTTGGATTTCAATGTGAGGCGG, crRNA2: AGTATACTCACGCCACCCACCGG, crRNA3: GACAAGCACCAGAAAGACCAGGG). Successfully edited cells were FACS sorted as MHCI non-expressing cells upon a 48-hour induction period with rmIFNγ (R&D Systems, 20 ng/mL).

Tumor challenge experiments

Tumor cells were cultured at 80% confluency before being dissociated using TrypLE (Gibco) enzyme mixture, washed, counted, and resuspended in PBS. Each mouse was injected subcutaneously in the lower back with 100 μL of cell suspension containing the appropriate number of cells (see each experiment for details). Tumor volume were determined according to the formula (57): $V = 0.4 \times L \times W^2$, where L=length, W=width of the tumor as measured by calipers.

Vector design and LV production

Immunogenic vectors: Minigenes encoding for viral epitopes (GP33: aaagctgtgtacaatttcgccaccatg; NP396: ttccaaccacaaaatgggcaatttata) were subcloned into a modified self-inactivating (SIN) and insulated lentiviral vector (CL20i4w-EF1a-GFP) under the control of the EF1a internal promoter. A stable monomeric form of mouse ubiquitin was attached directly upstream of the minigene to facilitate targeting of the peptide to the proteasomal pathway (58). The sequence encoding for the mCherry protein was attached

Author Manuscript Author Manuscript Author Manuscript Author Manuscript

downstream of the minigene through a P2A sequence to prevent the premature degradation of the fluorescent marker. VSV-G-pseudotyped viral particles were produced by using a 3rd generation packaging system as previously described (59).

Crispr vector: The S. pyogenes Cas9 gene and the sgRNA sequence were cloned into the CL20SF2-Cherry backbone plasmid under the internal control of the hybrid SF2/CMV and U6 promoters, respectively.

Dissociation and single cell preparation of human and mouse tumors.

The tumor tissue was mechanically minced into small pieces (2-3 mm), and subsequently subjected to enzymatic digestion by Collagenase 4 (Worthington Biochemical Co., 2 mg/mL) and Turbonuclease (Accelagen, 25 U/mL) for 30 min in RPMI 1640 medium supplemented with 5% FBS. Digested tumors were further dissociated by vigorous pipetting using wide bore tips and strained through a 70-μm cell strainer. The single cell suspension was depleted of RBC by using ammonium chloride isotonic lysis solution. The number of live cells is determined using a hemocytometer after exclusion of dead cells by Trypan blue dye.

Adoptive cell transfer

For most experiments that required analysis of P14 cells at day 7: Total splenocytes containing 5000 $GP33^{+}CD90.1^{+}CD8^{+}$ live T cells – isolated from naïve P14 $CD90.1^{+/+}$ mice, 8-10 weeks old, sex matched with the recipients – were injected intravenously via the retro orbital route into recipient mice at the indicated time points.

For priming experiment: Total $CD8^{+}$ T cells from naïve P14 C57Bl6 mice were negatively selected using magnetic beads (Miltenyi). Cells were then labeled with CTV (Invitrogen) at 5 μM final concentration for 5 min at RT. One-hundred thousand of live CTV-labeled $CD8^{+}$ T cells were adoptively transferred to each mouse.

Flow cytometry

Cell surface antigen staining was performed in FACS buffer (1xPBS supplemented with 2%FBS, 1-2mM EDTA, and 0.1% NaN_3) for 10-15 min at room temperature (RT). Subsequently cells were washed and finally fixed in 1% paraformaldehyde (PFA).

Tetramer generation: Monomers were obtained from the Yerkes NIH tetramer core facility and subsequently tetramerized using excess streptavidin-APC (Invitrogen), according to the protocol suggested by the tetramer core.

Flow cytometric analysis: Experimental flow data were acquired on a BD LSRII instrument operated through the BD FACSDiva V8 software. The raw flow data were analyzed using FCS Express 6 (De Novo Software). Immunophenotypic analysis of human tumor samples was based on samples that generated at least 100 cells/events on the parental gate represented on each graph, except for %TIM3 $CD8^{+}$ TILs for which the cutoff was set to 50 $PD1^{high}$ $CD8^{+}$ TILs.

Author Manuscript Author Manuscript Author Manuscript Author Manuscript

Ex vivo antigen stimulation of T cells and Intracellular cytokine staining (ICS) assay

To assess the ability of $CD8^+$ T cells to readily secrete effector cytokines, single cell suspensions from the indicated tissues were incubated with cognate peptide (1 μM) for 4 hours, at 37°C in a humidified CO_2 incubator. To enhance the signal of the produced cytokines, the protein transport inhibitors monensin and brefeldin A (BD biosciences; GolgiStop and GolgiPlug) were added at the start of culture at the recommended concentration by the manufacturer. The *ex vivo* stimulated cells were then stained for cell surface markers, fixed and permeabilized using CytoFix/CytoPerm kit (BD biosciences) as per the manufacturer's instructions, and finally stained with anti-IFNγ, anti-TNFα, and anti-IL-2 antibodies.

Antigen presentation assay

In Fig. S2: 100K $CD11b^+mCherry^+$ FACS purified myeloid cells from tumors were mixed with total naïve splenocytes containing 200K P14 $CD8^+$ T cells in a 96-well U-bottom cell culture plate, and co-incubated for 4 hours at 37°C in a CO_2 incubator.

In Fig. 4: $CD11b^+$ myeloid cells, that were positively selected using magnetic beads (Miltenyi) from young or adult tumors, were used ad APCs. The number of APCs was normalized to 100K $mCherry^+$ cells per well, in a 96-well flat-bottom cell culture plate. $CD8^+$ T cells from naïve P14 mice that were negatively selected using magnetic beads (Miltenyi) were used as responders at the indicated APC-to-P14 ratio. For proliferation assay shown in Fig. S6G, the purified $CD8^+$ T cells were labeled with CTV at 5 μM final concentration. Cells were incubated for 1 or 3 days as described at 37°C in a CO_2 incubator.

After the incubation period cell aggregates were disrupted and detached from the plate by adding 2 mM EDTA for 10 min at RT. The single cell suspension was stained for the indicated cell surface or intracellular markers and analyzed by flow cytometry. As positive control, naïve $CD8^+$ T cells were stimulated with 1 μM GP33 synthetic peptide.

Immunization

Soluble antigen (OVA protein): Young (4 weeks) or adult (24 weeks) mice were immunized with 20 μg OVA-AF488 (Invitrogen) emulsified in Complete Freund's Adjuvant (CFA; Sigma-Aldrich) at a 1:1 v/v ratio. Each mouse was injected subcutaneously (s.c.) with 100 μL of the protein emulsion. The draining lymph nodes (inguinal) were harvested 18 hours later and digested with collagenase IV and turbonuclease (see tumor dissociation protocol) to obtain a single cell suspension.

Intracellular antigen (apoptotic cells): Apoptosis was induced by incubating the tumor cells with 1μM staurosporin (Sigma) for 6 hours at 37°C in a humidified incubator. Ten million apoptotic cells were injected s.c. to each mouse, and the mCherry uptake by the APCs in the inguinal dLN was assessed the next day.

Single cell TCR repertoire analysis

For single cell TCR repertoire analysis cells were FACS index-sorted into a 96 well PCR plate preloaded with 2.5 μL of reverse transcription mixture per well (0.5 μL 5X VILO

Author Manuscript Author Manuscript Author Manuscript Author Manuscript

Reaction Mix, 0.25 μL 10X SuperScript Enzyme Mix (Invitrogen), 0.25 μL of 1% Triton X-100 (Sigma-Aldrich), and 1.5 μL nuclease free water). The CDR3α and β regions of each cell were amplified and sequenced using a nested, single-cell, multiplex PCR approach as previously described (60, 61). Sequences were parsed and characterized using the TCRdist pipeline (62).

DNA Methylation analysis

WGBS: Genomic DNA (gDNA) was extracted from the indicated sorted cells using a commercially available kit (Macherey-Nagel). Subsequently, less than 500 ng of gDNA was bisulfite (BS) treated to convert free cytosines to uracils using the EZ DNA Methylation-Gold (Zymo Research). The converted BS-DNA served as template to generate a DNA sequencing library using the TruSeq DNA Methylation Kit (Illumina). The library was sequenced using the Illumina HiSeq 2500 Sequencing System.

scRNA sequencing

Single-cell gene expression libraries were generated using the Chromium Single Cell 3' v2 kit (10X Genomics) with target outputs of 7,000-10,000 cells per library. Sequencing was performed on the Illumina NovaSeq platform with sufficient sequencing for at least 50,000 mean reads per cell. Raw sequencing data from each library were processed and aggregated using CellRanger (v3.0.2), normalizing for sequencing depth across libraries based on the median number of confidently mapped reads per cell. The subsequent feature/barcode matrices were then analyzed using Seurat (v3.1.0), controlling for potential variation owed to cell-specific variation including the number of unique RNA molecules, percent of mitochondrial gene expression, and inferred cell cycle state (63). Principal Component Analysis (PCA) was conducted on variable genes (detected using the standard 'vst' method), significant PCs were detected using random permutation, and those PCs were then leveraged for dimensional reduction and subsequent visualization using Uniform Manifold Approximation and Projection (UMAP) (64). To compare cells from distinct age groups, differential gene expression analysis was conducted using default parameters, and significantly up- or down-regulated genes for each condition were assessed for GO biological processes (v2020-07-16) and Reactome (v65) pathway enrichment using the PANTHER Overrepresentation Test (65).

Statistical analysis

Statistical analysis was performed using Prism V8 (GraphPad). The normal distribution of variables was calculated using Shapiro-Wilk test. The continuous variables with normal distribution are presented as mean ± standard deviation (SD), while variables with skewed distribution as median with interquartile range (IQR). Population means were calculated within a 95% confidential interval. Null hypothesis between means with normal distribution between the groups was tested by Student's t-test or one-way Anova parametric tests. Comparison of means without a normal distribution between the groups was done using Mann-Whitney U-test or Kruskal-Wallis nonparametric tests. Two-way Anova was performed to compare multiple categorical groups of 2 independent variables (factors). A two-tailed p-value of <0.05 is regarded as statistically significant, and different levels of

Author Manuscript Author Manuscript Author Manuscript Author Manuscript

significance are represented with asterisks: *P ≤ 0.05, **P ≤ 0.01, ***P ≤ 0.001, and ****P ≤ 0.0001.

Supplementary Material

Refer to Web version on PubMed Central for supplementary material.

Acknowledgements

We thank Richard Ashmun, PhD, and Flow Cytometry and Cell Sorting Shared Resource at SJCRH for cell sorting assistance; Jim Houston and the Developmental Neurobiology Flow Cytometry Core at SJCRH for cell sorting assistance; Brittney Gordon, B.S., RLAT for coordination of MAST tissue distribution; Vector Production and Development Laboratory at SJCRH for providing the backbone lentiviral vectors (CL20SF2-Cherry and CL20i4w-EF1a-GFP) used in this study.

Funding:

This work was supported by American Lebanese Syrian Associated Charities, ALSAC, (to BY); National Institutes of Health grants 1R01AI114442 & 1R01CA237311 (to BY); Immune Tolerance Network grant UM1AI109565 (to BY); NIH grants 1R01AI107625 and 1R01AI136514 (to PT); Key For a Cure Foundation (to BY and PT); SJCRH DBSTP and HMP Garwood Fellowship (to AM and AEZ respectively); and the National Cancer Institute of the National Institutes of Health under Award Number P30 CA021765 (to SJCRH Hartwell center for sequencing services and to PT for Developmental Funds). E.S. is supported by the St Baldrick's Foundation and National Comprehensive Cancer Network. The content is solely the responsibility of the authors and does not necessarily represent the official views of the National Institutes of Health.

References

1. Vigano S, Utzschneider DT, Perreau M, Pantaleo G, Zehn D, Harari A, Functional avidity: a measure to predict the efficacy of effector T cells? Clin Dev Immunol 2012, 153863 (2012). [PubMed: 23227083]
2. Zehn D, King C, Bevan MJ, Palmer E, TCR signaling requirements for activating T cells and for generating memory. Cell Mol Life Sci 69, 1565–1575 (2012). [PubMed: 22527712]
3. Gettinger SN, Choi J, Mani N, Sanmamed MF, Datar I, Sowell R, Du VY, Kaftan E, Goldberg S, Dong W, Zelterman D, Politi K, Kavathas P, Kaech S, Yu X, Zhao H, Schlessinger J, Lifton R, Rimm DL, Chen L, Herbst RS, Schalper KA, A dormant TIL phenotype defines non-small cell lung carcinomas sensitive to immune checkpoint blockers. Nat Commun 9, 3196 (2018). [PubMed: 30097571]
4. Im SJ, Hashimoto M, Gerner MY, Lee J, Kissick HT, Burger MC, Shan Q, Hale JS, Lee J, Nasti TH, Sharpe AH, Freeman GJ, Germain RN, Nakaya HI, Xue HH, Ahmed R, Defining CD8+ T cells that provide the proliferative burst after PD-1 therapy. Nature 537, 417–421 (2016). [PubMed: 27501248]
5. Utzschneider DT, Charmoy M, Chennupati V, Pousse L, Ferreira DP, Calderon-Copete S, Danilo M, Alfei F, Hofmann M, Wieland D, Pradervand S, Thimme R, Zehn D, Held W, T Cell Factor 1-Expressing Memory-like CD8(+) T Cells Sustain the Immune Response to Chronic Viral Infections. Immunity 45, 415–427 (2016). [PubMed: 27533016]
6. Miller BC, Sen DR, Al Abosy R, Bi K, Virkud YV, LaFleur MW, Yates KB, Lako A, Felt K, Naik GS, Manos M, Gjini E, Kuchroo JR, Ishizuka JJ, Collier JL, Griffin GK, Maleri S, Comstock DE, Weiss SA, Brown FD, Panda A, Zimmer MD, Manguso RT, Hodi FS, Rodig SJ, Sharpe AH, Haining WN, Subsets of exhausted CD8(+) T cells differentially mediate tumor control and respond to checkpoint blockade. Nat Immunol 20, 326–336 (2019). [PubMed: 30778252]
7. Chen Z, Ji Z, Ngiow SF, Manne S, Cai Z, Huang AC, Johnson J, Staupe RP, Bengsch B, Xu C, Yu S, Kurachi M, Herati RS, Vella LA, Baxter AE, Wu JE, Khan O, Beltra JC, Giles JR, Stelekati E, McLane LM, Lau CW, Yang X, Berger SL, Vahedi G, Ji H, Wherry EJ, TCF-1-Centered Transcriptional Network Drives an Effector versus Exhausted CD8 T Cell-Fate Decision. Immunity, (2019).

Author Manuscript Author Manuscript Author Manuscript Author Manuscript

8. Danilo M, Chennupati V, Silva JG, Siegert S, Held W, Suppression of Tcf1 by Inflammatory Cytokines Facilitates Effector CD8 T Cell Differentiation. Cell Rep 22, 2107–2117 (2018). [PubMed: 29466737]

9. Yao C, Sun HW, Lacey NE, Ji Y, Moseman EA, Shih HY, Heuston EF, Kirby M, Anderson S, Cheng J, Khan O, Handon R, Reilley J, Fioravanti J, Hu J, Gossa S, Wherry EJ, Gattinoni L, McGavern DB, O'Shea JJ, Schwartzberg PL, Wu T, Single-cell RNA-seq reveals TOX as a key regulator of CD8(+) T cell persistence in chronic infection. Nat Immunol 20, 890–901 (2019). [PubMed: 31209400]

10. Seo H, Chen J, Gonzalez-Avalos E, Samaniego-Castruita D, Das A, Wang YH, Lopez-Moyado IF, Georges RO, Zhang W, Onodera A, Wu CJ, Lu LF, Hogan PG, Bhandoola A, Rao A, TOX and TOX2 transcription factors cooperate with NR4A transcription factors to impose CD8(+) T cell exhaustion. Proc Natl Acad Sci U S A 116, 12410–12415 (2019). [PubMed: 31152140]

11. Scott AC, Dundar F, Zumbo P, Chandran SS, Klebanoff CA, Shakiba M, Trivedi P, Menocal L, Appleby H, Camara S, Zamarin D, Walther T, Snyder A, Femia MR, Comen EA, Wen HY, Hellmann MD, Anandasabapathy N, Liu Y, Altorki NK, Lauer P, Levy O, Glickman MS, Kaye J, Betel D, Philip M, Schietinger A, TOX is a critical regulator of tumour-specific T cell differentiation. Nature 571, 270–274 (2019). [PubMed: 31207604]

12. Khan O, Giles JR, McDonald S, Manne S, Ngiow SF, Patel KP, Werner MT, Huang AC, Alexander KA, Wu JE, Attanasio J, Yan P, George SM, Bengsch B, Staupe RP, Donahue G, Xu W, Amaravadi RK, Xu X, Karakousis GC, Mitchell TC, Schuchter LM, Kaye J, Berger SL, Wherry EJ, TOX transcriptionally and epigenetically programs CD8(+) T cell exhaustion. Nature 571, 211–218 (2019). [PubMed: 31207603]

13. Alfei F, Kanev K, Hofmann M, Wu M, Ghoneim HE, Roelli P, Utzschneider DT, von Hoesslin M, Cullen JG, Fan Y, Eisenberg V, Wohlleber D, Steiger K, Merkler D, Delorenzi M, Knolle PA, Cohen CJ, Thimme R, Youngblood B, Zehn D, TOX reinforces the phenotype and longevity of exhausted T cells in chronic viral infection. Nature 571, 265–269 (2019). [PubMed: 31207605]

14. Pereira LF, de Souza AP, Borges TJ, Bonorino C, Impaired in vivo CD4+ T cell expansion and differentiation in aged mice is not solely due to T cell defects: decreased stimulation by aged dendritic cells. Mech Ageing Dev 132, 187–194 (2011). [PubMed: 21453718]

15. Grolleau-Julius A, Harning EK, Abernathy LM, Yung RL, Impaired dendritic cell function in aging leads to defective antitumor immunity. Cancer Res 68, 6341–6349 (2008). [PubMed: 18676859]

16. Chougnet CA, Thacker RI, Shehata HM, Hennies CM, Lehn MA, Lages CS, Janssen EM, Loss of Phagocytic and Antigen Cross-Presenting Capacity in Aging Dendritic Cells Is Associated with Mitochondrial Dysfunction. J Immunol 195, 2624–2632 (2015). [PubMed: 26246142]

17. Crooke SN, Ovsyannikova IG, Poland GA, Kennedy RB, Immunosenescence and human vaccine immune responses. Immun Ageing 16, 25 (2019). [PubMed: 31528180]

18. Park JA, Cheung NV, Limitations and opportunities for immune checkpoint inhibitors in pediatric malignancies. Cancer Treat Rev 58, 22–33 (2017). [PubMed: 28622628]

19. Grobner SN, Worst BC, Weischenfeldt J, Buchhalter I, Kleinheinz K, Rudneva VA, Johann PD, Balasubramanian GP, Segura-Wang M, Brabetz S, Bender S, Hutter B, Sturm D, Pfaff E, Hubschmann D, Zipprich G, Heinold M, Eils J, Lawerenz C, Erkek S, Lambo S, Waszak S, Blattmann C, Borkhardt A, Kuhlen M, Eggert A, Fulda S, Gessler M, Wegert J, Kappler R, Baumhoer D, Burdach S, Kirschner-Schwabe R, Kontny U, Kulozik AE, Lohmann D, Hettmer S, Eckert C, Bielack S, Nathrath M, Niemeyer C, Richter GH, Schulte J, Siebert R, Westermann F, Molenaar JJ, Vassal G, Witt H, Project IP-S, Project IM-S, Burkhardt B, Kratz CP, Witt O, van Tilburg CM, Kramm CM, Fleischhack G, Dirksen U, Rutkowski S, Fruhwald M, von Hoff K, Wolf S, Klingebiel T, Koscielniak E, Landgraf P, Koster J, Resnick AC, Zhang J, Liu Y, Zhou X, Waanders AJ, Zwijnenburg DA, Raman P, Brors B, Weber UD, Northcott PA, Pajtler KW, Kool M, Piro RM, Korbel JO, Schlesner M, Eils R, Jones DTW, Lichter P, Chavez L, Zapatka M, Pfister SM, The landscape of genomic alterations across childhood cancers. Nature 555, 321–327 (2018). [PubMed: 29489754]

20. Ma X, Liu Y, Liu Y, Alexandrov LB, Edmonson MN, Gawad C, Zhou X, Li Y, Rusch MC, Easton J, Huether R, Gonzalez-Pena V, Wilkinson MR, Hermida LC, Davis S, Sioson E, Pounds S, Cao X, Ries RE, Wang Z, Chen X, Dong L, Diskin SJ, Smith MA, Guidry Auvil JM, Meltzer PS, Lau CC, Perlman EJ, Maris JM, Meshinchi S, Hunger SP, Gerhard DS, Zhang J, Pan-cancer genome and

Author Manuscript Author Manuscript Author Manuscript Author Manuscript

transcriptome analyses of 1,699 paediatric leukaemias and solid tumours. Nature 555, 371–376 (2018). [PubMed: 29489755]

21. Zamora AE, Crawford JC, Allen EK, Guo XJ, Bakke J, Carter RA, Abdelsamed HA, Moustaki A, Li Y, Chang TC, Awad W, Dallas MH, Mullighan CG, Downing JR, Geiger TL, Chen T, Green DR, Youngblood BA, Zhang J, Thomas PG, Pediatric patients with acute lymphoblastic leukemia generate abundant and functional neoantigen-specific CD8(+) T cell responses. Sci Transl Med 11, (2019).
22. Subudhi SK, Vence L, Zhao H, Blando J, Yadav SS, Xiong Q, Reuben A, Aparicio A, Corn PG, Chapin BF, Pisters LL, Troncoso P, Tidwell RS, Thall P, Wu CJ, Zhang J, Logothetis CL, Futreal A, Allison JP, Sharma P, Neoantigen responses, immune correlates, and favorable outcomes after ipilimumab treatment of patients with prostate cancer. Sci Transl Med 12, (2020).
23. Lopez-Otin C, Blasco MA, Partridge L, Serrano M, Kroemer G, The hallmarks of aging. Cell 153, 1194–1217 (2013). [PubMed: 23746838]
24. Schietinger A, Philip M, Krisnawan VE, Chiu EY, Delrow JJ, Basom RS, Lauer P, Brockstedt DG, Knoblaugh SE, Hammerling GJ, Schell TD, Garbi N, Greenberg PD, Tumor-Specific T Cell Dysfunction Is a Dynamic Antigen-Driven Differentiation Program Initiated Early during Tumorigenesis. Immunity 45, 389–401 (2016). [PubMed: 27521269]
25. Pircher H, Burki K, Lang R, Hengartner H, Zinkernagel RM, Tolerance induction in double specific T-cell receptor transgenic mice varies with antigen. Nature 342, 559–561 (1989). [PubMed: 2573841]
26. Lin H, Wei S, Hurt EM, Green MD, Zhao L, Vatan L, Szeliga W, Herbst R, Harms PW, Fecher LA, Vats P, Chinnaiyan AM, Lao CD, Lawrence TS, Wicha M, Hamanishi J, Mandai M, Kryczek I, Zou W, Host expression of PD-L1 determines efficacy of PD-L1 pathway blockade-mediated tumor regression. J Clin Invest 128, 805–815 (2018). [PubMed: 29337305]
27. Tang H, Liang Y, Anders RA, Taube JM, Qiu X, Mulgaonkar A, Liu X, Harrington SM, Guo J, Xin Y, Xiong Y, Nham K, Silvers W, Hao G, Sun X, Chen M, Hannan R, Qiao J, Dong H, Peng H, Fu YX, PD-L1 on host cells is essential for PD-L1 blockade-mediated tumor regression. J Clin Invest 128, 580–588 (2018). [PubMed: 29337303]
28. Eickhoff S, Brewitz A, Gerner MY, Klauschen F, Komander K, Hemmi H, Garbi N, Kaisho T, Germain RN, Kastenmuller W, Robust Anti-viral Immunity Requires Multiple Distinct T Cell-Dendritic Cell Interactions. Cell 162, 1322–1337 (2015). [PubMed: 26296422]
29. Prlic M, Williams MA, Bevan MJ, Requirements for CD8 T-cell priming, memory generation and maintenance. Curr Opin Immunol 19, 315–319 (2007). [PubMed: 17433873]
30. McAdam AJ, Schweitzer AN, Sharpe AH, The role of B7 co-stimulation in activation and differentiation of CD4+ and CD8+ T cells. Immunol Rev 165, 231–247 (1998). [PubMed: 9850864]
31. Greenfield EA, Nguyen KA, Kuchroo VK, CD28/B7 costimulation: a review. Crit Rev Immunol 18, 389–418 (1998). [PubMed: 9784967]
32. Boada-Romero E, Martinez J, Heckmann BL, Green DR, The clearance of dead cells by efferocytosis. Nat Rev Mol Cell Biol 21, 398–414 (2020). [PubMed: 32251387]
33. Saeki H, Moore AM, Brown MJ, Hwang ST, Cutting edge: secondary lymphoid-tissue chemokine (SLC) and CC chemokine receptor 7 (CCR7) participate in the emigration pathway of mature dendritic cells from the skin to regional lymph nodes. J Immunol 162, 2472–2475 (1999). [PubMed: 10072485]
34. Schittenhelm L, Hilkens CM, Morrison VL, beta2 Integrins As Regulators of Dendritic Cell, Monocyte, and Macrophage Function. Front Immunol 8, 1866 (2017). [PubMed: 29326724]
35. Curiel TJ, Wei S, Dong H, Alvarez X, Cheng P, Mottram P, Krzysiek R, Knutson KL, Daniel B, Zimmermann MC, David O, Burow M, Gordon A, Dhurandhar N, Myers L, Berggren R, Hemminki A, Alvarez RD, Emilie D, Curiel DT, Chen L, Zou W, Blockade of B7-H1 improves myeloid dendritic cell-mediated antitumor immunity. Nat Med 9, 562–567 (2003). [PubMed: 12704383]
36. Latchman YE, Liang SC, Wu Y, Chernova T, Sobel RA, Klemm M, Kuchroo VK, Freeman GJ, Sharpe AH, PD-L1-deficient mice show that PD-L1 on T cells, antigen-presenting cells, and

Author Manuscript Author Manuscript Author Manuscript Author Manuscript

host tissues negatively regulates T cells. Proc Natl Acad Sci U S A 101, 10691–10696 (2004). [PubMed: 15249675]

37. Kratochvill F, Neale G, Haverkamp JM, Van de Velde LA, Smith AM, Kawauchi D, McEvoy J, Roussel MF, Dyer MA, Qualls JE, Murray PJ, TNF Counterbalances the Emergence of M2 Tumor Macrophages. Cell Rep 12, 1902–1914 (2015). [PubMed: 26365184]
38. Rath M, Muller I, Kropf P, Closs EI, Munder M, Metabolism via Arginase or Nitric Oxide Synthase: Two Competing Arginine Pathways in Macrophages. Front Immunol 5, 532 (2014). [PubMed: 25386178]
39. Mills CD, Ley K, M1 and M2 macrophages: the chicken and the egg of immunity. J Innate Immun 6, 716–726 (2014). [PubMed: 25138714]
40. Varesio L, Down regulation of RNA labeling as a selective marker for cytotoxic but not suppressor macrophages. J Immunol 132, 2683–2685 (1984). [PubMed: 6202756]
41. Stewart E, Federico SM, Chen X, Shelat AA, Bradley C, Gordon B, Karlstrom A, Twarog NR, Clay MR, Bahrami A, Freeman BB 3rd, Xu B, Zhou X, Wu J, Honnell V, Ocarz M, Blankenship K, Dapper J, Mardis ER, Wilson RK, Downing J, Zhang J, Easton J, Pappo A, Dyer MA, Orthotopic patient-derived xenografts of paediatric solid tumours. Nature 549, 96–100 (2017). [PubMed: 28854174]
42. Downing JR, Wilson RK, Zhang J, Mardis ER, Pui CH, Ding L, Ley TJ, Evans WE, The Pediatric Cancer Genome Project. Nat Genet 44, 619–622 (2012). [PubMed: 22641210]
43. Wherry EJ, Ha SJ, Kaech SM, Haining WN, Sarkar S, Kalia V, Subramaniam S, Blattman JN, Barber DL, Ahmed R, Molecular signature of CD8+ T cell exhaustion during chronic viral infection. Immunity 27, 670–684 (2007). [PubMed: 17950003]
44. Scheper W, Kelderman S, Fanchi LF, Linnemann C, Bendle G, de Rooij MAJ, Hirt C, Mezzadra R, Slagter M, Dijkstra K, Kluin RJC, Snaebjornsson P, Milne K, Nelson BH, Zijlmans H, Kenter G, Voest EE, Haanen J, Schumacher TN, Low and variable tumor reactivity of the intratumoral TCR repertoire in human cancers. Nat Med 25, 89–94 (2019). [PubMed: 30510250]
45. Li H, van der Leun AM, Yofe I, Lubling Y, Gelbard-Solodkin D, van Akkooi ACJ, van den Braber M, Rozeman EA, Haanen J, Blank CU, Horlings HM, David E, Baran Y, Bercovich A, Lifshitz A, Schumacher TN, Tanay A, Amit I, Dysfunctional CD8 T Cells Form a Proliferative, Dynamically Regulated Compartment within Human Melanoma. Cell 176, 775–789 e718 (2019). [PubMed: 30595452]
46. Majzner RG, Simon JS, Grosso JF, Martinez D, Pawel BR, Santi M, Merchant MS, Geoerger B, Hezam I, Marty V, Vielh P, Daugaard M, Sorensen PH, Mackall CL, Maris JM, Assessment of programmed death-ligand 1 expression and tumor-associated immune cells in pediatric cancer tissues. Cancer 123, 3807–3815 (2017). [PubMed: 28608950]
47. Linehan E, Fitzgerald DC, Ageing and the immune system: focus on macrophages. Eur J Microbiol Immunol (Bp) 5, 14–24 (2015). [PubMed: 25883791]
48. Linehan E, Dombrowski Y, Snoddy R, Fallon PG, Kissenpfennig A, Fitzgerald DC, Aging impairs peritoneal but not bone marrow-derived macrophage phagocytosis. Aging Cell 13, 699–708 (2014). [PubMed: 24813244]
49. Noy R, Pollard JW, Tumor-associated macrophages: from mechanisms to therapy. Immunity 41, 49–61 (2014). [PubMed: 25035953]
50. Hesketh M, Sahin KB, West ZE, Murray RZ, Macrophage Phenotypes Regulate Scar Formation and Chronic Wound Healing. Int J Mol Sci 18, (2017).
51. Smith NL, Wissink E, Wang J, Pinello JF, Davenport MP, Grimson A, Rudd BD, Rapid proliferation and differentiation impairs the development of memory CD8+ T cells in early life. J Immunol 193, 177–184 (2014). [PubMed: 24850719]
52. Huseby ES, Sather B, Huseby PG, Goverman J, Age-dependent T cell tolerance and autoimmunity to myelin basic protein. Immunity 14, 471–481 (2001). [PubMed: 11336692]
53. Jimenez O, Barros MH, De Matteo E, Garcia Lombardi M, Preciado MV, Niedobitek G, Chabay P, M1-like macrophage polarization prevails in young children with classic Hodgkin Lymphoma from Argentina. Sci Rep 9, 12687 (2019). [PubMed: 31481738]

Author Manuscript Author Manuscript Author Manuscript Author Manuscript

54. Faul F, Erdfelder E, Lang AG, Buchner A, G*Power 3: a flexible statistical power analysis program for the social, behavioral, and biomedical sciences. Behav Res Methods 39, 175–191 (2007). [PubMed: 17695343]
55. Faul F, Erdfelder E, Buchner A, Lang AG, Statistical power analyses using G*Power 3.1: tests for correlation and regression analyses. Behav Res Methods 41, 1149–1160 (2009). [PubMed: 19897823]
56. Rusch M, Nakitandwe J, Shurtleff S, Newman S, Zhang Z, Edmonson MN, Parker M, Jiao Y, Ma X, Liu Y, Gu J, Walsh MF, Becksfort J, Thrasher A, Li Y, McMurry J, Hedlund E, Patel A, Easton J, Yergeau D, Vadodaria B, Tatevossian RG, Raimondi S, Hedges D, Chen X, Hagiwara K, McGee R, Robinson GW, Klco JM, Gruber TA, Ellison DW, Downing JR, Zhang J, Clinical cancer genomic profiling by three-platform sequencing of whole genome, whole exome and transcriptome. Nat Commun 9, 3962 (2018). [PubMed: 30262806]
57. Tomayko MM, Reynolds CP, Determination of subcutaneous tumor size in athymic (nude) mice. Cancer Chemother Pharmacol 24, 148–154 (1989). [PubMed: 2544306]
58. Rodriguez F, Zhang J, Whitton JL, DNA immunization: ubiquitination of a viral protein enhances cytotoxic T-lymphocyte induction and antiviral protection but abrogates antibody induction. J Virol 71, 8497–8503 (1997). [PubMed: 9343207]
59. Hanawa H, Hematti P, Keyvanfar K, Metzger ME, Krouse A, Donahue RE, Kepes S, Gray J, Dunbar CE, Persons DA, Nienhuis AW, Efficient gene transfer into rhesus repopulating hematopoietic stem cells using a simian immunodeficiency virus-based lentiviral vector system. Blood 103, 4062–4069 (2004). [PubMed: 14976042]
60. Dash P, McClaren JL, Oguin TH 3rd, Rothwell W, Todd B, Morris MY, Becksfort J, Reynolds C, Brown SA, Doherty PC, Thomas PG, Paired analysis of TCRalpha and TCRbeta chains at the single-cell level in mice. J Clin Invest 121, 288–295 (2011). [PubMed: 21135507]
61. Dash P, Wang GC, Thomas PG, Single-Cell Analysis of T-Cell Receptor alphabeta Repertoire. Methods Mol Biol 1343, 181–197 (2015). [PubMed: 26420718]
62. Dash P, Fiore-Gartland AJ, Hertz T, Wang GC, Sharma S, Souquette A, Crawford JC, Clemens EB, Nguyen THO, Kedzierska K, La Gruta NL, Bradley P, Thomas PG, Quantifiable predictive features define epitope-specific T cell receptor repertoires. Nature 547, 89–93 (2017). [PubMed: 28636592]
63. Tirosh I, Izar B, Prakadan SM, Wadsworth MH 2nd, Treacy D, Trombetta JJ, Rotem A, Rodman C, Lian C, Murphy G, Fallahi-Sichani M, Dutton-Regester K, Lin JR, Cohen O, Shah P, Lu D, Genshaft AS, Hughes TK, Ziegler CG, Kazer SW, Gaillard A, Kolb KE, Villani AC, Johannessen CM, Andreev AY, Van Allen EM, Bertagnolli M, Sorger PK, Sullivan RJ, Flaherty KT, Frederick DT, Jane-Valbuena J, Yoon CH, Rozenblatt-Rosen O, Shalek AK, Regev A, Garraway LA, Dissecting the multicellular ecosystem of metastatic melanoma by single-cell RNA-seq. Science 352, 189–196 (2016). [PubMed: 27124452]
64. McInnes L, J. H.; Melville J, UMAP: Uniform Manifold Approximation and Projection for Dimension Reduction. arXiv:1802.03426, (2018).
65. Mi H, Muruganujan A, Huang X, Ebert D, Mills C, Guo X, Thomas PD, Protocol Update for large-scale genome and gene function analysis with the PANTHER classification system (v.14.0). Nat Protoc 14, 703–721 (2019). [PubMed: 30804569]
66. Brand L. A. Amy, Altman Micah, Hlava Marjorie, Scott Jo, Beyondauthorship: Attribution, contribution, collaboration, and credit. Learned Publishing 28, 151–155 (2015).
67. Edgar R, Domrachev M, Lash AE, Gene Expression Omnibus: NCBI gene expression and hybridization array data repository. Nucleic Acids Res 30, 207–210 (2002). [PubMed: 11752295]

Author Manuscript Author Manuscript Author Manuscript Author Manuscript

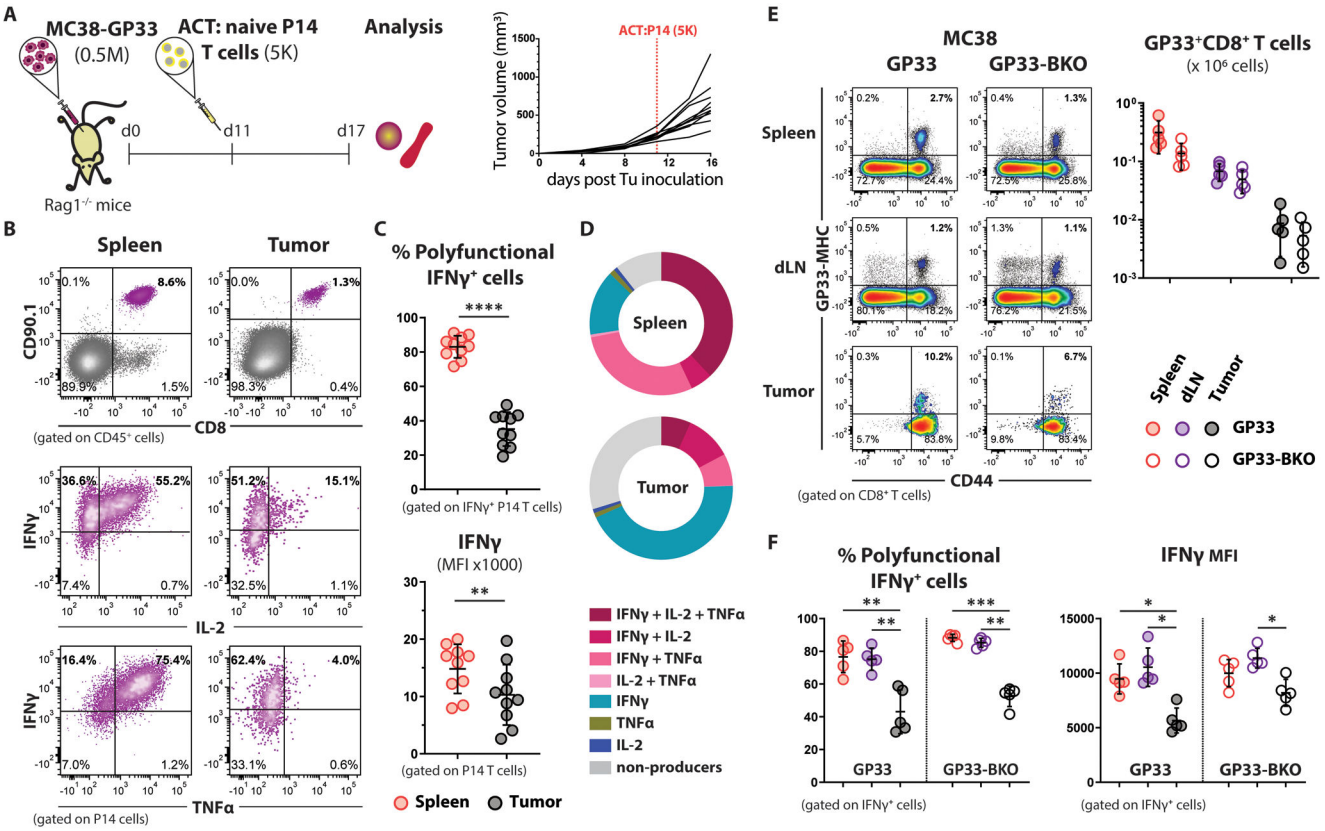

Figure 1. Antigen cross-presentation by the TME is sufficient to enforce the tumor-associated dysfunctional state of CD8$^+$ T cells.

(**A**) Schematic experimental design for panels (B-D): 5000 naïve P14 CD8$^+$ T cells were adoptively transferred to TB Rag1$^{-/-}$ mice (n=10), and their functionality was analyzed one week after transfer.

(**B**) Representative flow cytometry dot plots from the indicated tissues of TB mice showing the expression of GP33-specific TCRs on the surface of adoptively transferred P14 CD8$^+$ T cells (upper row), and their potential to produce cytokines upon *ex vivo* stimulation with cognate peptide (2 bottom rows).

(**C**) Statistical analysis of the cytokine profile shown in (B). Percent polyfunctionality is calculated as the percentage of IFNγ producing P14 cells that also co-produce TNFα or IL-2. Mean ±SD; paired Welch t-test.

(**D**) Functional composition of CD8$^+$ T cells is summarized in the pie charts, which are color-coded according to the polyfunctionality of CD8$^+$ T cells.

(**E**) Representative flow cytometry density plots showing the frequency of endogenous GP33-specific CD8$^+$ T cells in the spleen, dLN, and tumors from MC38-GP33 (MHCI-proficient) and MC38-GP33-BKO (MHCI-deficient) TB mice at effector stage (day 7). The absolute cell counts of GP33-specific CD8$^+$ T cells isolated from the indicated tissues of TB mice (n=5 per experimental group) are plotted on the right. Mean ±SD; multiple unpaired Welch t-test.

Author Manuscript Author Manuscript Author Manuscript Author Manuscript

(**F**) Impaired cytokine response of tumor infiltrating $CD8^+$ T cells generated against MC38-GP33 tumor cells deficient or sufficient in MHCI expression (n=5). Mean ±SD; two-way Anova with Tukey correction.

A *p*-value of <0.05 is regarded as statistically significant, and different levels of significance are represented with asterisks: *P ≤ 0.05, **P ≤ 0.01, ***P ≤ 0.001, and ****P ≤ 0.0001.

Author Manuscript Author Manuscript Author Manuscript Author Manuscript

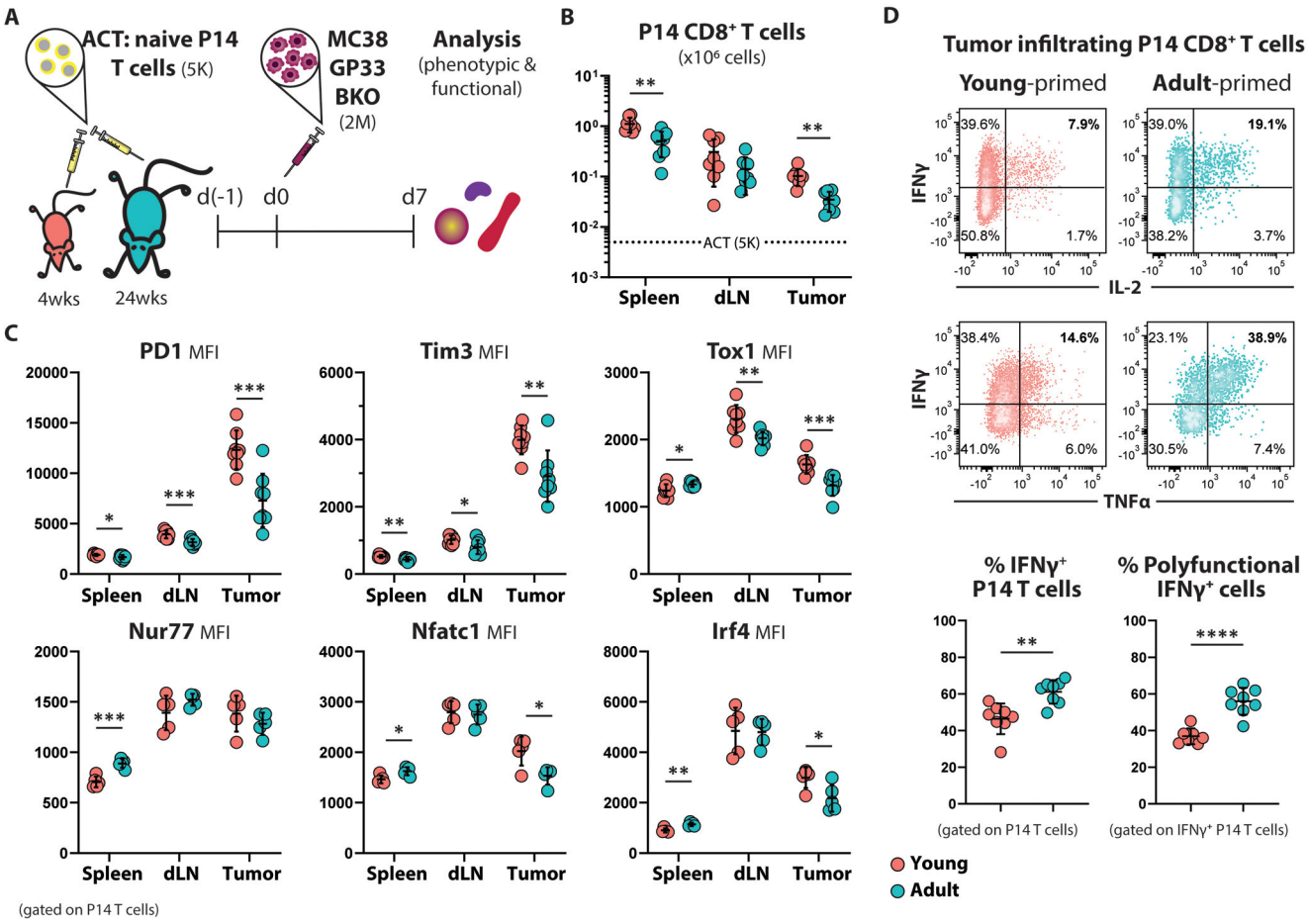

Figure 2. Increased frequency of terminally differentiated antigen-specific CD8$^+$ T cells in young TB hosts.

(**A**) Schematic experimental design: Five thousand naïve CD90.1$^+$ P14 CD8$^+$ T cells were adoptively transferred into young (4-weeks old; n=8) and adult (24-weeks old; n=8) C57Bl6 mice. One day later all mice were subcutaneously challenged with MC38-GP33-BKO cells. Phenotypic and functional analysis was performed 7 days post tumor challenge.

(**B**) Summarized data showing the expansion of transferred P14 CD8$^+$ T cells as total cell count in the indicated organs. Mean ±SD; multiple unpaired Welch t-test.

(**C**) Summarized data showing the expression intensity of the indicated proteins in P14 CD8$^+$ T cells residing in the spleens, dLNs, and tumors of young and adult hosts. Mean ±SD; multiple unpaired Welch t-test.

(**D**) Representative flow cytometry density plots (left) and summarized data (right) showing cytokine production by young- and adult-primed P14 TILs upon 4h *ex vivo* stimulation with GP33 peptide. Mean ±SD; multiple unpaired Welch t-test.

A *p*-value of <0.05 is regarded as statistically significant, and different levels of significance are represented with asterisks: *P ≤ 0.05, **P ≤ 0.01, ***P ≤ 0.001, and ****P ≤ 0.0001.

Author Manuscript Author Manuscript Author Manuscript Author Manuscript

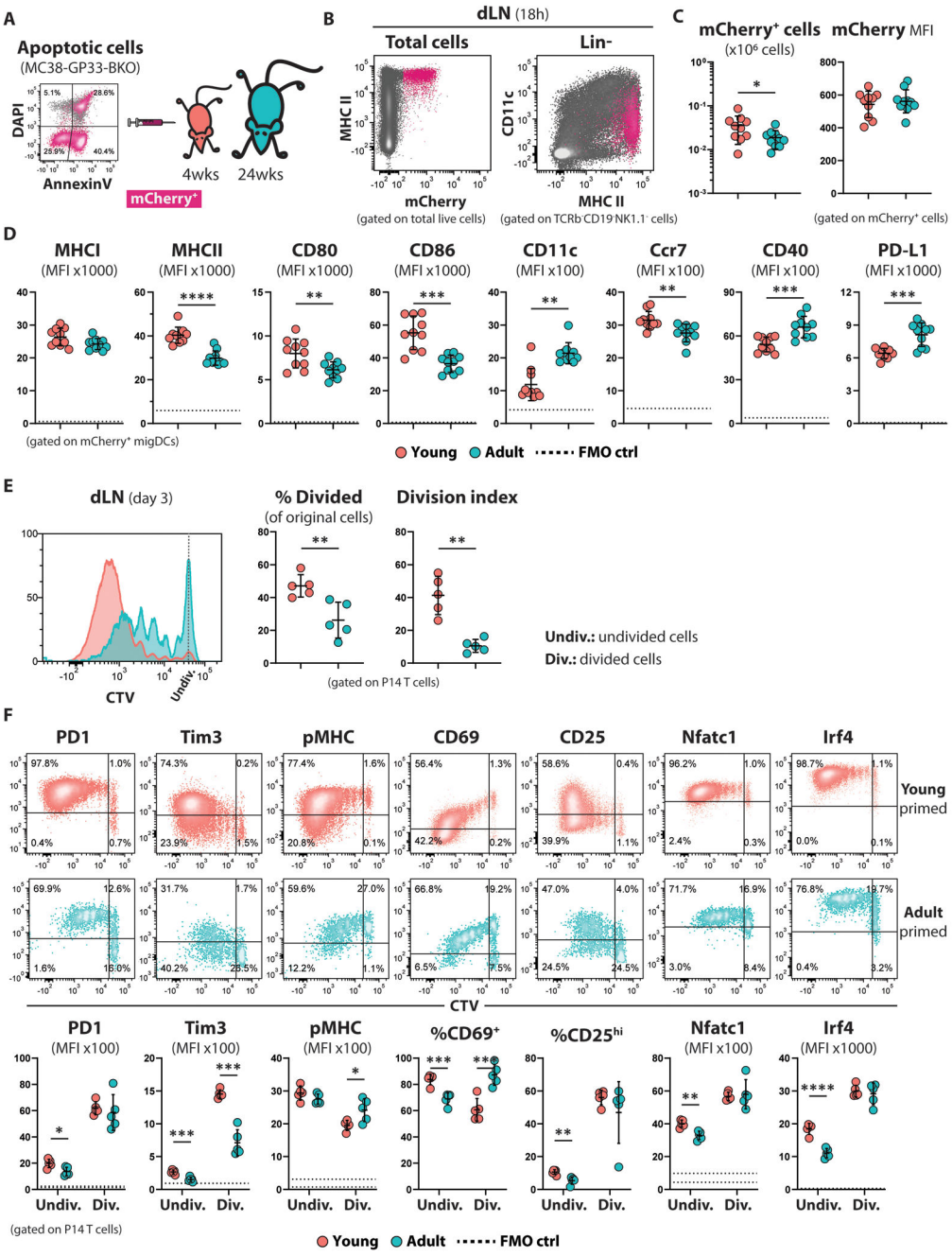

Figure 3. The enhanced activated phenotype of the young-primed CD8$^+$ T cells is established early during their stimulation in dLNs.

(**A**) Schematic experimental design for panels (B-D): Young (4-weeks old; n=10) and adult (24-weeks old; n=10) C57Bl6 mice were inoculated s.c. with apoptotic MC38-GP33-BKO cells, and the APCs present in the draining lymph nodes were analyzed 18 hours later.

(**B**) Representative flow cytometry plots showing the mCherry$^+$ uptake by cells in the dLN of young or adult mice.

(**C**) Summarized data showing the total number of mCherry$^+$ cells in dLNs and their mCherry fluorescent intensity. Mean ±SD; unpaired Welch t-test.

Author Manuscript Author Manuscript Author Manuscript Author Manuscript

(**D**) Summarized data showing the expression intensity of DC markers involved in maturation and migration of mCherry$^+$ mDCs from the dLNs of young and adult mice. The dotted line represents the autofluoresence of the corresponding channel calculated from FMO control samples. Mean ±SD; unpaired Welch t-test.

(**E**) CTV-labeled P14 CD8$^+$ T (100K) were adoptively transferred in young and adult mice (n=5 per group) one day before they were challenged with MHCI-deficient MC38-GP33 cells. Proliferation of P14 cells based on CTV dilution was calculated 3 days upon tumor challenge in the dLNs. Mean ±SD; unpaired Welch t-test.

(**F**) Expression profiles of the indicated proteins in divided (Div.) and undivided (Undiv.) P14 CD8$^+$ T cells primed for 3 days in young or adult TB mice. Representative density plots (top) and summarized data (bottom) are shown. The dotted lines on each graph representing MFI indicate the autofluorescence of the divided (upper line) and undivided (lower line) cells. Mean ±SD; multiple unpaired Welch t-test.

A *p*-value of <0.05 is regarded as statistically significant, and different levels of significance are represented with asterisks: *P ≤ 0.05, **P ≤ 0.01, ***P ≤ 0.001, and ****P ≤ 0.0001.

Author Manuscript Author Manuscript Author Manuscript Author Manuscript

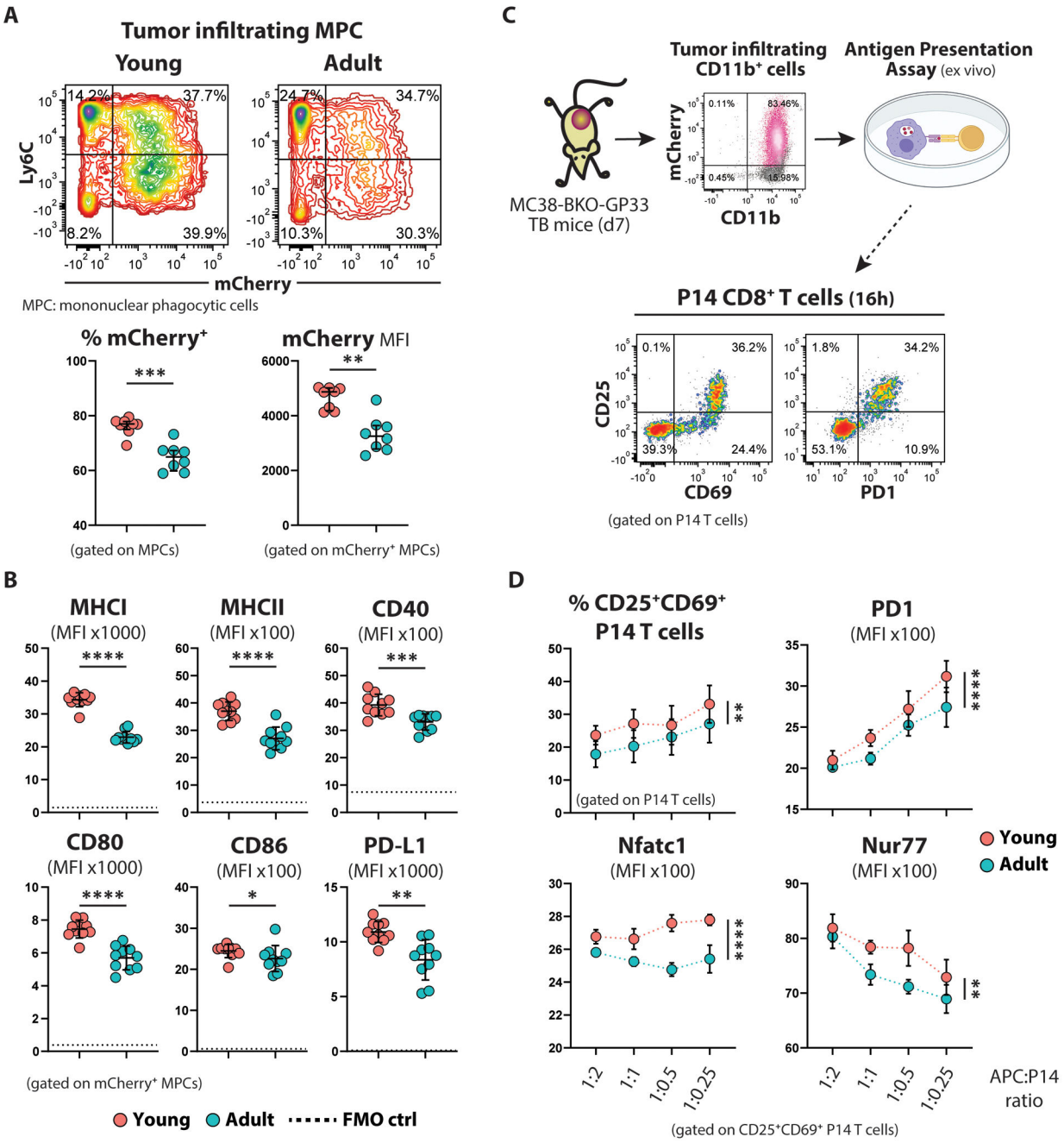

Figure 4. Young tumor infiltrating MPCs are more efficient at cross-presenting tumor antigens.

(**A**) Representative flow cytometry contour plots (top) and summarized data (bottom; n=8 per group) showing the tumor mCherry uptake by tumor infiltrating mononuclear phagocytotic cells (MPCs). Mean ±SD; unpaired Welch t-test.

(**B**) Summarized data showing the expression intensity of MHC molecules and costimulatory molecules on the surface of mCherry^{+} MPCs from young and adult TB mice. The dotted lines represent the autofluorescence calculated based on FMO control samples. Mean ±SD; unpaired Welch t-test.

Author Manuscript Author Manuscript Author Manuscript Author Manuscript

(**C**) Schematic experimental design of the antigen cross-presentation assay: $CD11b^+$ myeloid cells isolated from young or adult tumors and normalized for the number of $mCherry^+$ cells were used to stimulate naïve P14 cells ex vivo. Activation of P14 cells was assessed the next day.
(**D**) Summarized data (n=5 per group) showing the percentage of activated ($CD69^+CD25^+$) P14 $CD8^+$ T cells and the expression level of the indicated markers by the activated subset, at different APC:P14 ratios. Mean ±SD; two-way Anova with Sidak correction.
A *p*-value of <0.05 is regarded as statistically significant, and different levels of significance are represented with asterisks: *P ≤ 0.05, **P ≤ 0.01, ***P ≤ 0.001, and ****P ≤ 0.0001.

Author Manuscript Author Manuscript Author Manuscript Author Manuscript

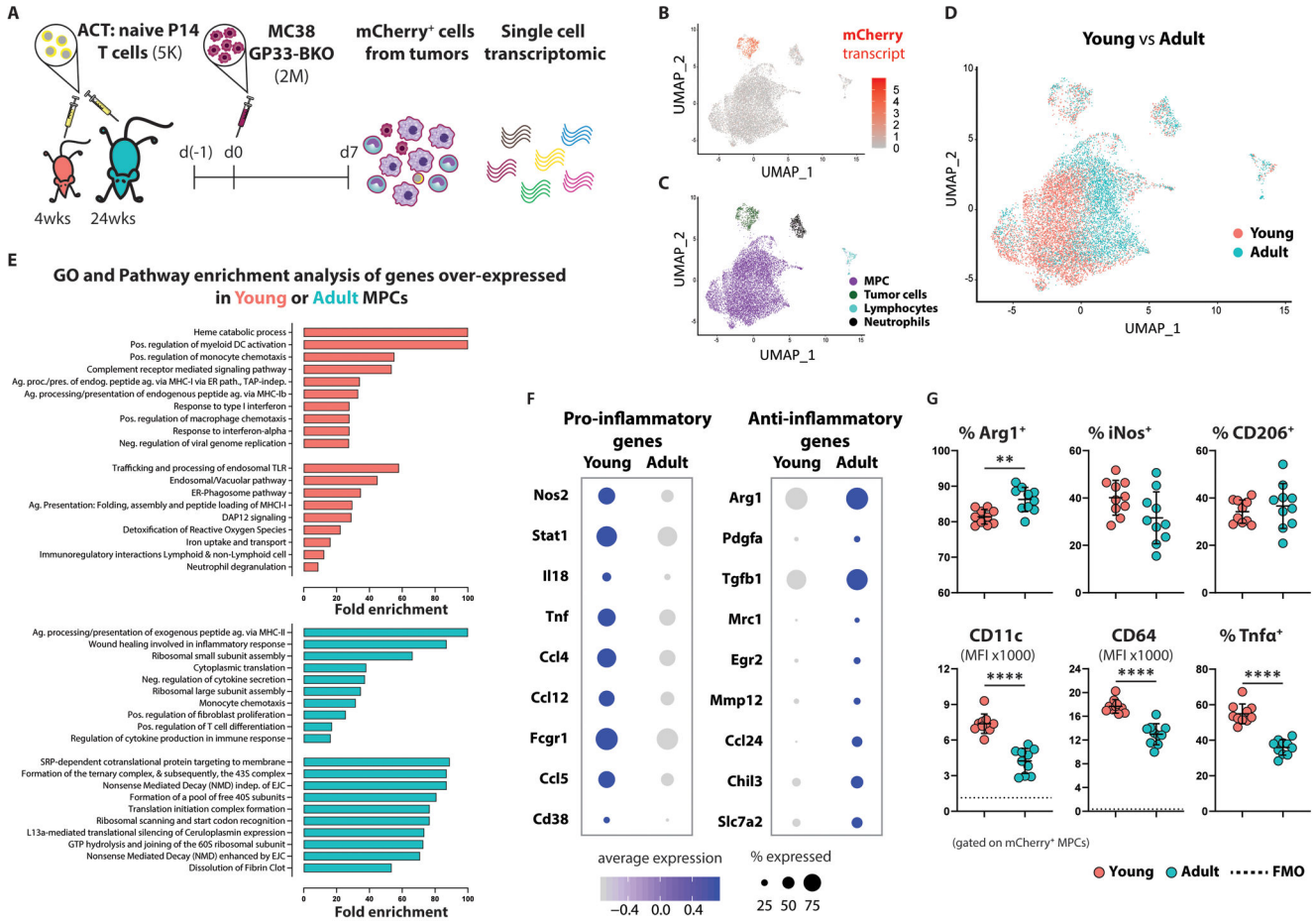

Figure 5. Young tumor infiltrating MPCs are skewed toward a pro-inflammatory phenotype.

(**A**) Schematic experimental design for isolating antigen^{+} tumor-associated immune cells.

(**B**) Single-cell gene expression plot featuring log-scaled mCherry expression levels, which clearly distinguishes tumor from non-tumor cells. Data were projected using Uniform Manifold Approximation and Projection (UMAP) as described in the methods**** (pooled data from 5 mice per experimental group). The experiment was repeated twice with similar results.

(**C**) Single-cell gene expression analyses revealed distinct clusters corresponding to tumor cells, neutrophils, lymphocytes, and a composite of other myeloid-derived tumor-infiltrating cells (MPCs).

(**D**) Single-cell gene expression plot with individual cells colored according to the age of their host. Although tumor cells showed no clear evidence of gene expression differences between young and adult cells owing to host age, the majority composite of infiltrating myeloid cells showed extreme gene expression heterogeneity as a function of host age.

(**E**) Gene ontology (biological processes) and pathway enrichment analysis of genes overexpressed in young (top) or adult (bottom) MPCs. Top 10 enriched terms are presented.

(**F**) Dot plots representing the average expression of, and percentage of cells expressing, markers commonly used to distinguish pro-inflammatory and anti-inflammatory macrophages. The size of a given dot corresponds to the proportion of cells within the

Author Manuscript Author Manuscript Author Manuscript Author Manuscript

respective group expressing it in any amount, whereas color encodes average expression scaled across all groups presented (an expression value of −1 indicates one standard deviation below the mean).

(**G**) Summarized data (n=10 per group) showing the expression of proteins associated with polarization of macrophages. Mean ±SD; unpaired Welch t-test.

A *p*-value of <0.05 is regarded as statistically significant, and different levels of significance are represented with asterisks: *P ≤ 0.05, **P ≤ 0.01, ***P ≤ 0.001, and ****P ≤ 0.0001.

Author Manuscript Author Manuscript Author Manuscript Author Manuscript

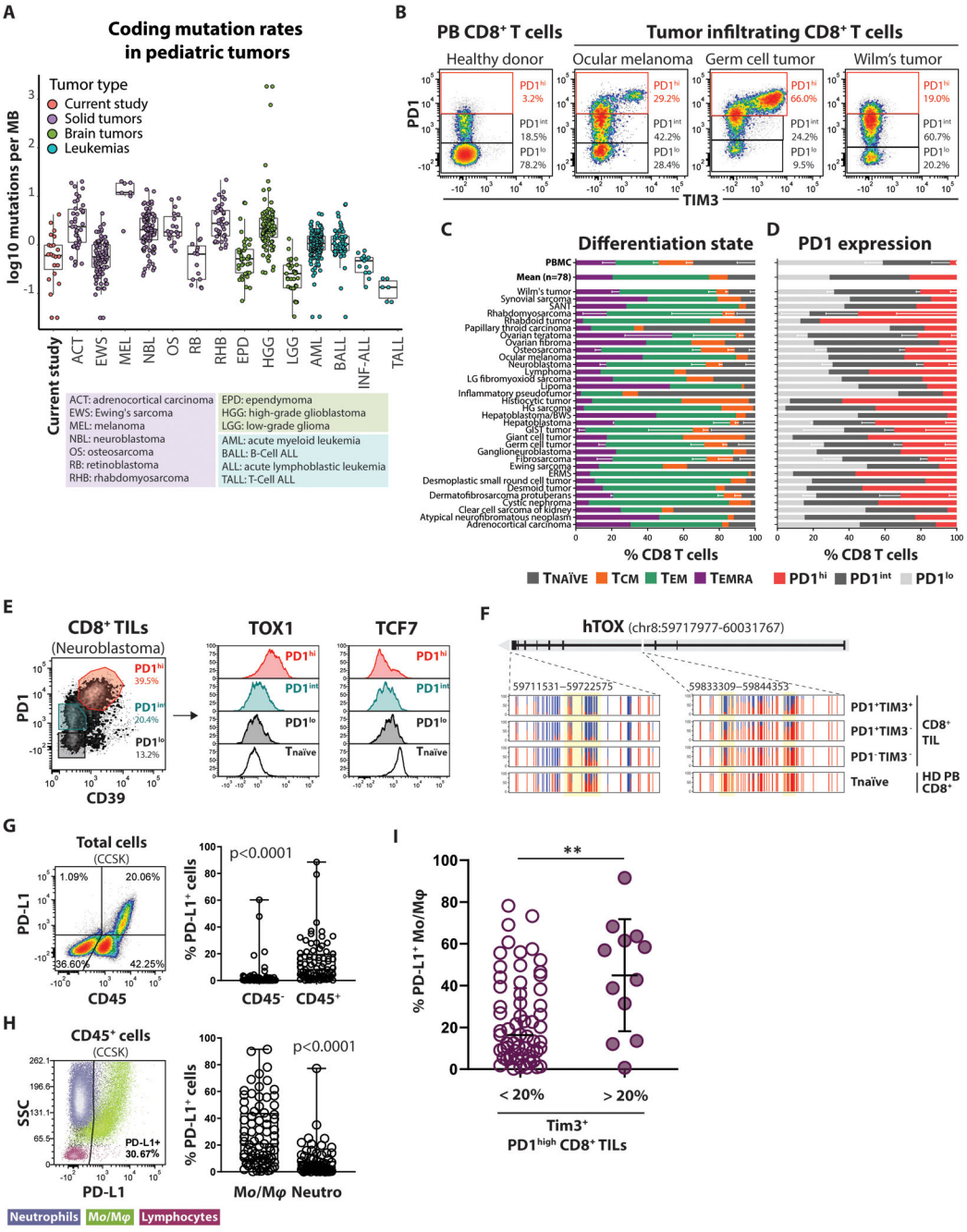

Figure 6. Pediatric solid tumors are infiltrated by antigen-experienced CD8$^+$ T cells despite their low mutational burden.

(**A**) Mutation rates of a subset (n=23) of the tumors utilized in this study for which whole exome sequencing data were available compared to the mutation rates of common pediatric tumors previously published as a part of the Pediatric Cancer Genome Project. Mutation rates were calculated as the number of coding mutations per megabase of sufficiently covered genome sequence and are plotted in log10 scale due to the extreme range observed in some HGG tumors.

Author Manuscript Author Manuscript Author Manuscript Author Manuscript

(**B**) Representative flow cytometry density plots showing variable expression levels of inhibitory receptors, PD1 and TIM3, on tumor infiltrating $CD8^+$ T cells compared to peripheral blood $CD8^+$ T cells from a healthy donor.
(**C**) Summarized data for naïve and memory subset phenotypes of $CD8^+$ T cells isolated from pediatric tumors (n=78). Naïve = $CCR7^+CD45RO^-$, central memory (Tcm) = $CCR7^+CD45RO^+$, effector memory (Tem) = $CCR7^-CD45RO^-$, Temra = $CCR7^-CD45RO^-$.
(**D**) Summarized data of PD1 expression on $CD8^+$ T cells isolated from pediatric tumors (n=78) and peripheral blood $CD8^+$ T cells from healthy donors (n=4).
(**E**) Histogram FACS plots showing the fluorescence intensity of TOX1 and TCF7 among $PD1^{hi}$, PD^{int}, and $PD1^{lo}$ $CD8^+$ TIL subsets (as defined on the right density plot) from a Neuroblastoma sample. Tnaïve ($CCR7^+CD45RO^-$) from the peripheral blood of a healthy donor is used as reference (black line).
(**F**) WGBS nucleotide-resolution view of TOX1 locus among different subsets of $CD8^+$ TILs isolated from a Germ cell tumor sample, and $CD8^+$ T naïve cells from the peripheral blood of a healthy donor. Each vertical line represents a single CpG cite, the red segment indicates the percentage of methylated reads, while the blue segment indicates the percentage of non-methylated reads for the same CpG site.
(**G**) Representative flow cytometry density plot (left) and summarized data (right) of the frequency of PD-L1 expressing cells among $CD45^-$ and $CD45^+$ immune infiltrates in pediatric solid tumors (n=83). Mean ±SD; paired nonparametric Wilcoxon test.
(**H**) Representative flow cytometry dot plot (left), and summarized data (right) showing that tumor infiltrating monocytes/macrophages are the main source of PD-L1 expression in pediatric solid tumors (n=79). Mean ±SD; paired nonparametric Wilcoxon test.
(**I**) Frequency of PD-L1 expressing tumor-associated monocytes/macrophages among tumors with low (< 20%) and high (> 20%) prevalence of $TIM3^+$ $PD1^{high}$ $CD8^+$ T cells. Mean ±SD; unpaired nonparametric Mann Whitney test.
A *p*-value of <0.05 is regarded as statistically significant, and different levels of significance are represented with asterisks: *P ≤ 0.05, **P ≤ 0.01, ***P ≤ 0.001, and ****P ≤ 0.0001.